TU2A001

Charge Selector Challenges in High Power Heavy Ion Linacs

Alexander Plastun

Accelerator Staff Physicist

18 August 2026

This material is based upon work supported by the U.S. Department of Energy, Office of Science, Office of Nuclear Physics and used resources of the Facility for Rare Isotope Beams (FRIB) Operations, which is a DOE Office of Science User Facility under Award Number DE-SC0023633.

What is FRIB?

- **F**acility for **R**are **I**sotope **B**eams, at Michigan State University, USA
- U.S. Department of Energy Office of Science **U**ser **F**acility
- In-flight **isotope production** on a thin graphite target

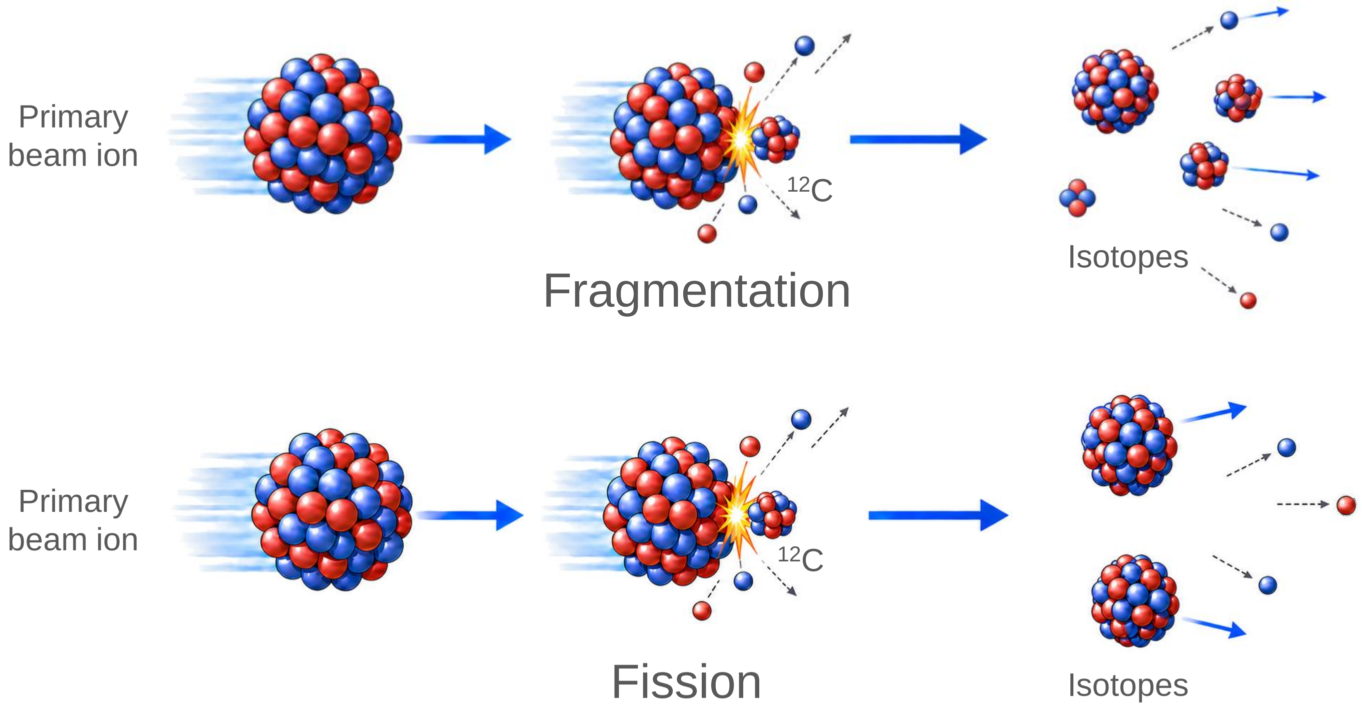

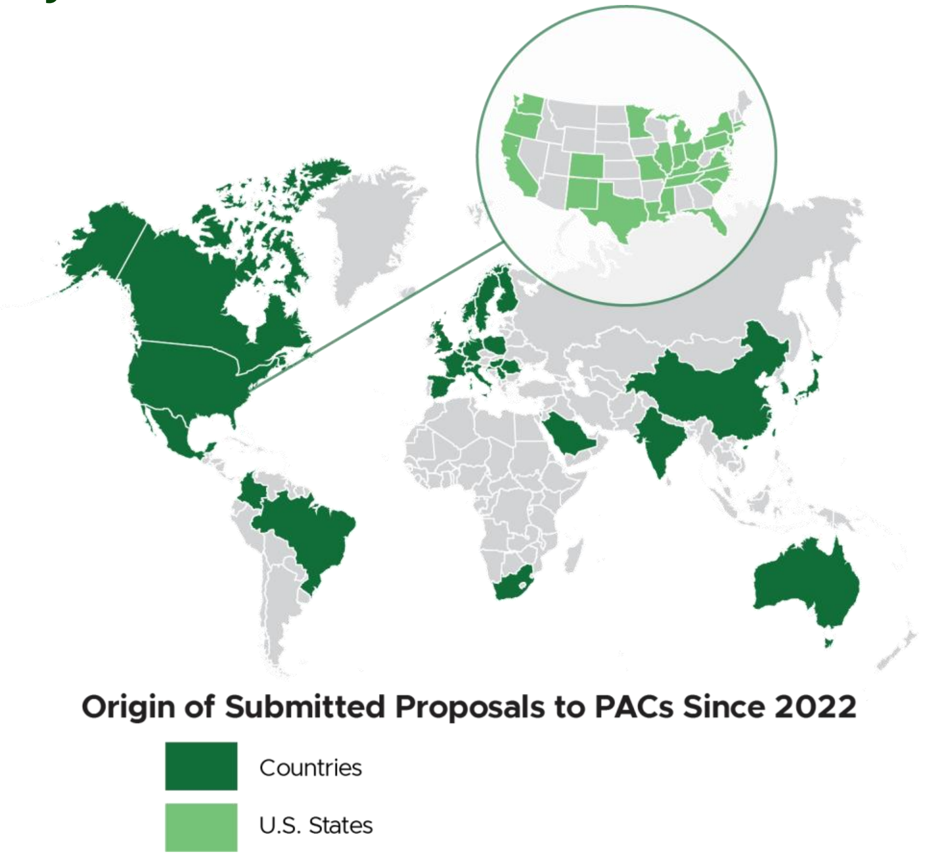

FRIB Linac – World's Highest Power Heavy Ion Accelerator

- Continuous-wave (CW) Superconducting RF linac
- Current power level: **20** kW
- Demonstrated: **30** kW of ^{238}U on Oct. 16, 2025
- Goal: **400** kW

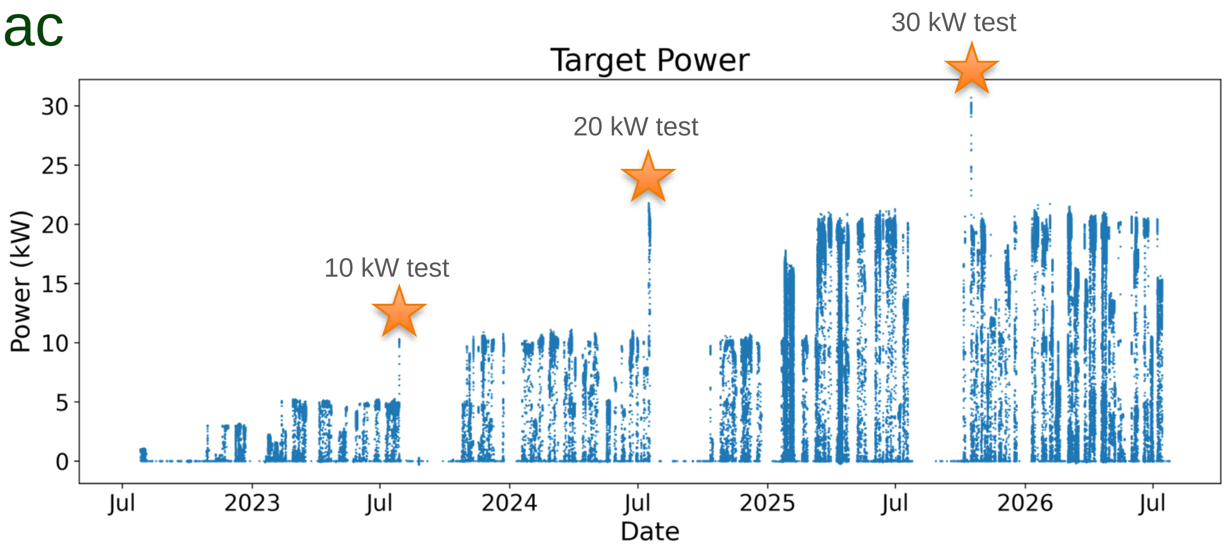

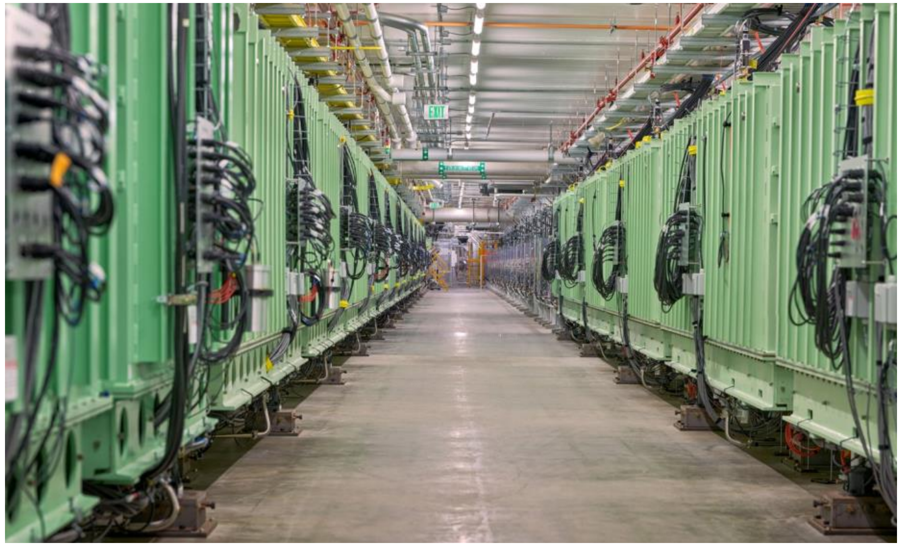

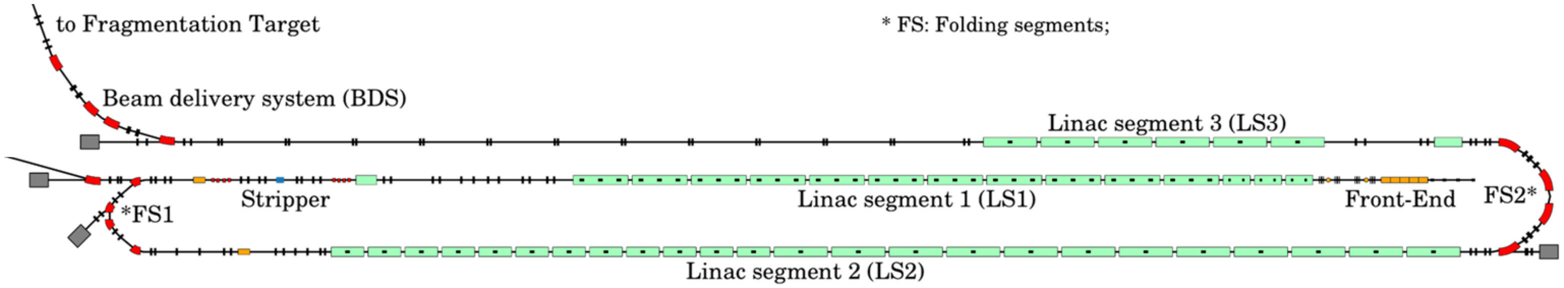

Challenging Operations

- Started user operation in May 2022
- Over **4000** hours per year
- Above **93%** availability

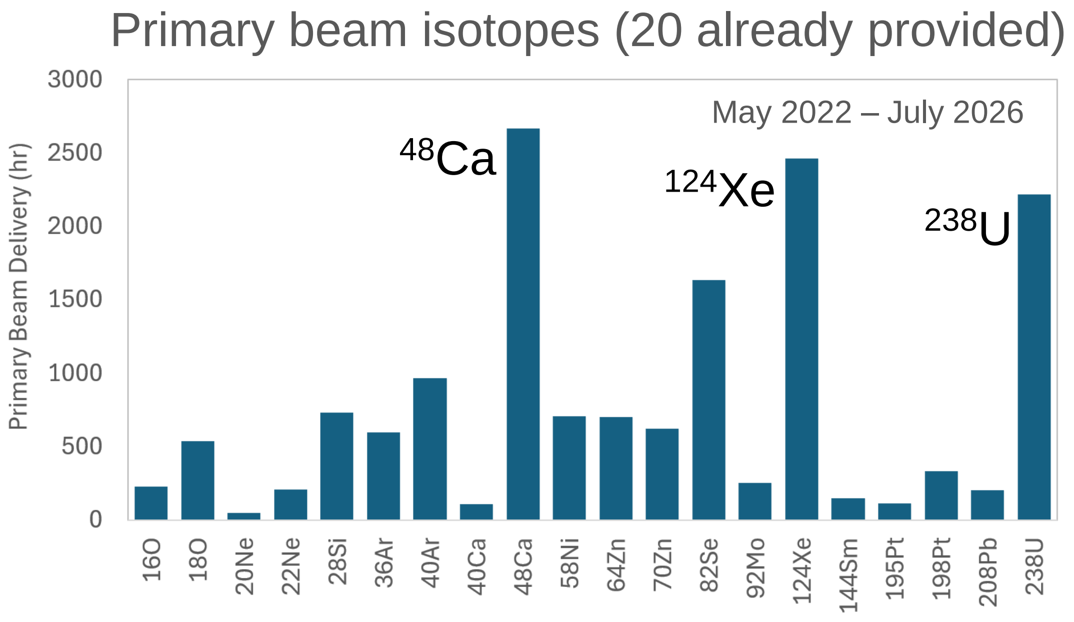

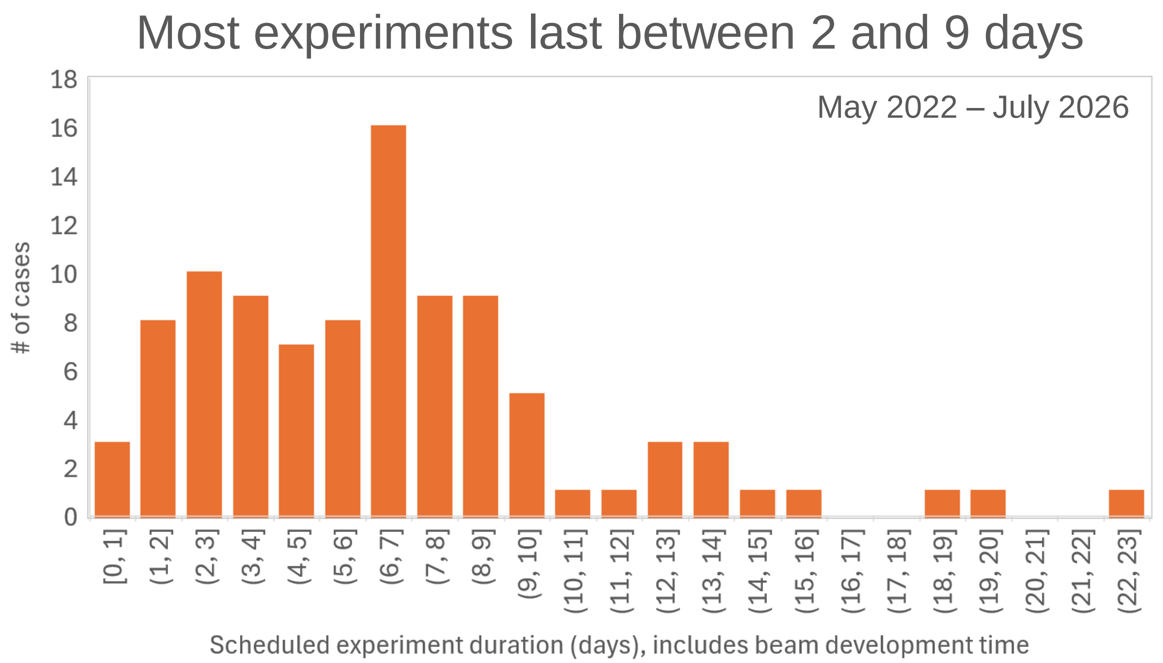

Stripping Boosts Energy Gain

- Energy gain **balance** between pre-stripper and post-stripper:

$$\Delta W = Q_{init}(U_{str}) + Q_{str}(U_{tot} - U_{str})$$

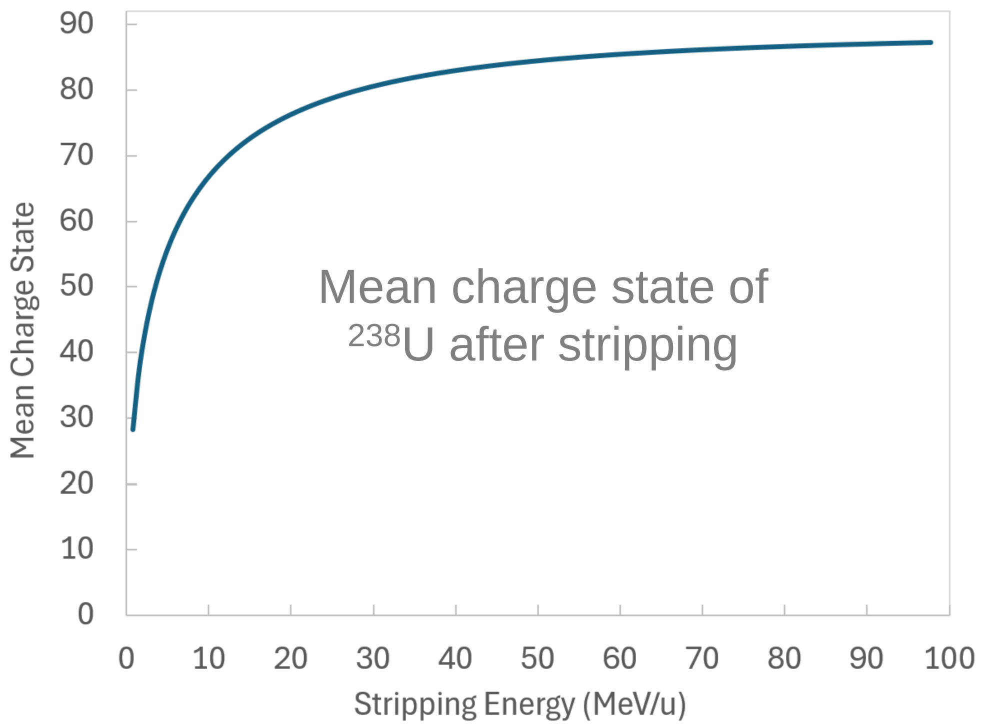

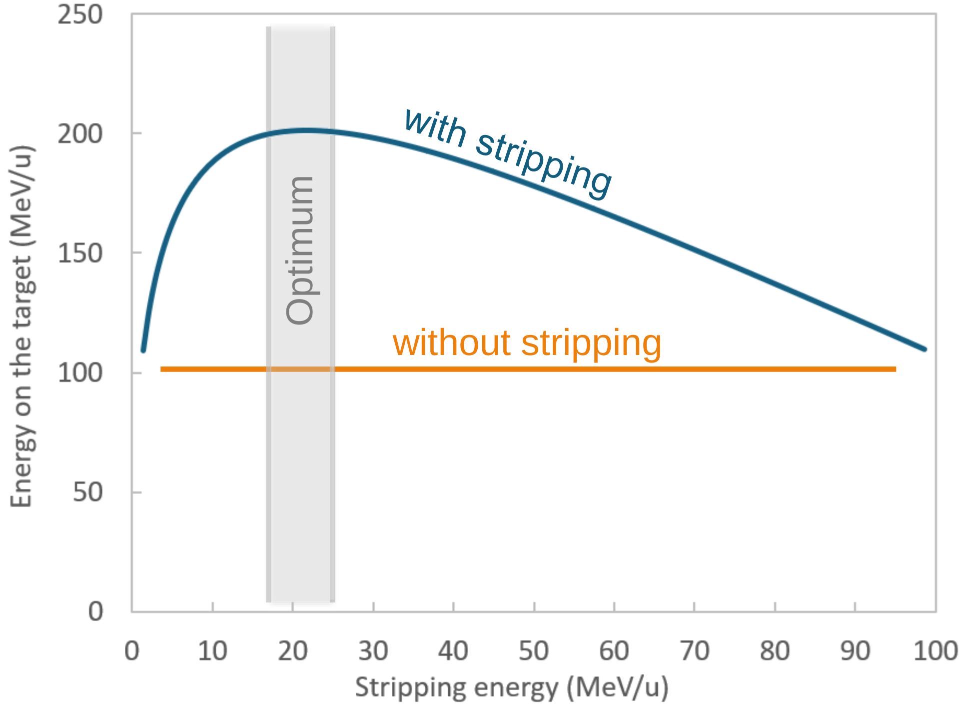

Liquid Lithium Charge Stripper

- Carbon **foils** is a **conventional** material for charge stripping
  - But it could not survive heavy ion irradiation long enough
  - Experienced some thermal management issues (upgraded since then)
- **Liquid lithium** stripper, unique design for high-power accelerators
  - In use since 2023, no power limit reached so far
  - Lithium circulation hours reached over **17,000 hours** without any critical incidents

Rotating carbon foil (1 mg/cm^2)

[T. Kanemura, et al., PHYSICAL REVIEW LETTERS 128, 212301 (2022)]

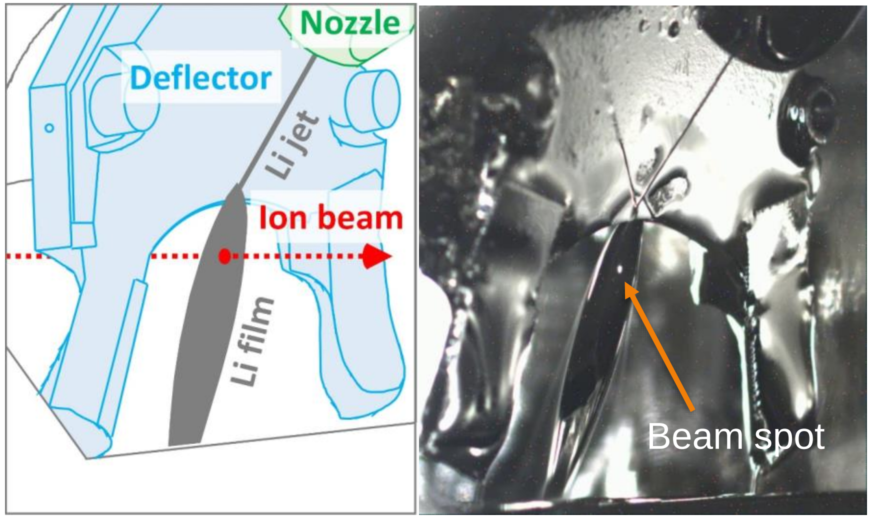

Li film during 30 kW ^{238}U beam test in Oct. 2025

Charge-Exchange Equilibrium

- Stripping into multiple charge states due to a competition between electron **loss** and **capture**

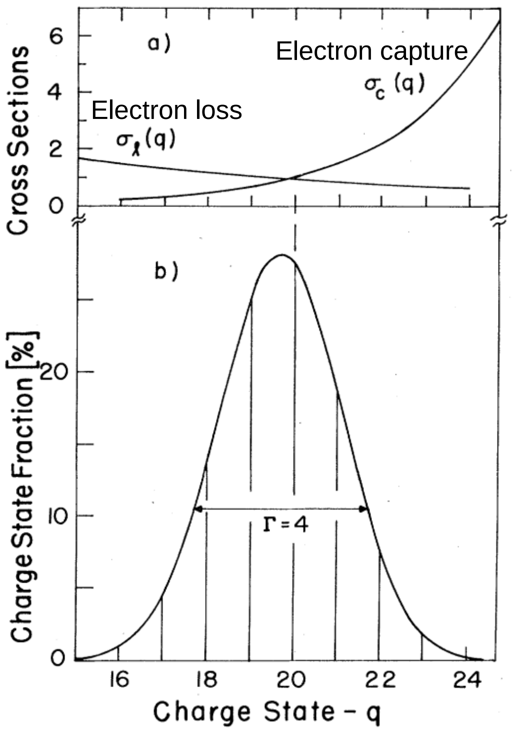

FIG. 2.3. (a) Hypothetical cross sections for capture and loss of a single electron, taken from Eq. (2.10) with $b_c = 0.4$, $b_l = 0.1$, and $q_x = 20$; (b) corresponding Gaussian equilibrium charge state distribution which is centered symmetrically around $q_0 = 19.7$ and has a width $d_0 = 1.43$.

[H.D. Betz, REVIEWS OF MODERN PHYSICS 44, 8, 1972]

Let us assume that cross sections for capture and loss of a single electron can be represented by curves of exponential form

$$\sigma(q, q-1) = A_c \exp[b_c(q-q_0)],$$
$$\sigma(q, q+1) = A_l \exp[-b_l(q-q_0)]. \qquad (2.10)$$

Provided that we choose $A_c = A_l \exp[(b_l - b_c)/2]$, it can be shown (Bell, 1953) that Eq. (2.10) yields a Gaussian equilibrium distribution around q_0,

$$F(q) = (2\pi d^2)^{-1/2} \exp[-(q-q_0)^2/(2d^2)], \qquad (2.11)$$

where the width depends only on the sum of the two parameters b_c and b_l,

$$d = (b_c + b_l)^{-1/2}. \qquad (2.12)$$

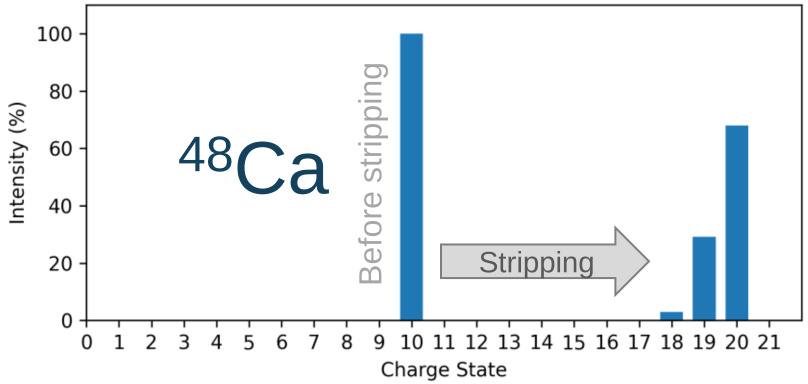

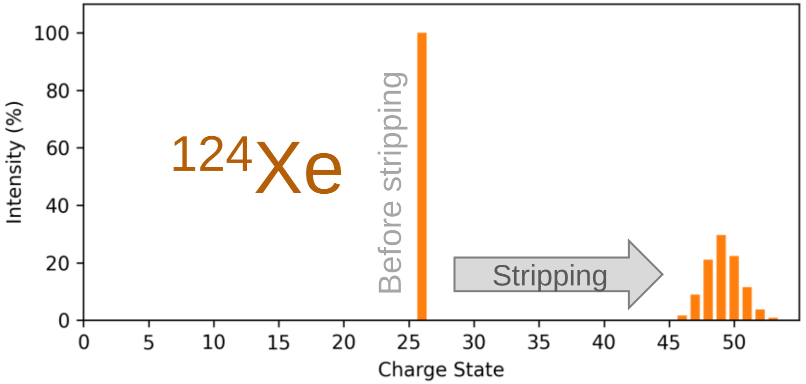

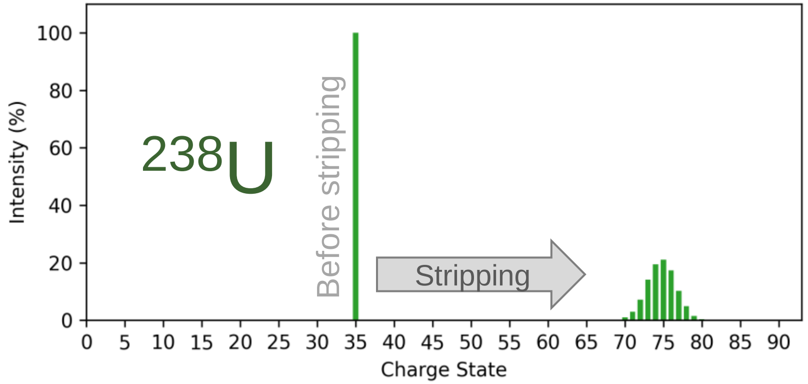

Multi-charge-state Acceleration

- Unlike cyclotrons, linear accelerators can accept and accelerate several charge states
  - Discussed in 1960s for UNILAC, at GSI [1]
  - Demonstrated at Argonne National Laboratory in 2000 [2]
  - Utilized at FRIB since 2020 [3]
    - » Demonstrated acceleration, in 2020
    - » Isotope **production**, since 2022

FRIB linac acceptance:

$$\frac{\Delta Q}{Q} < \pm 3\%$$

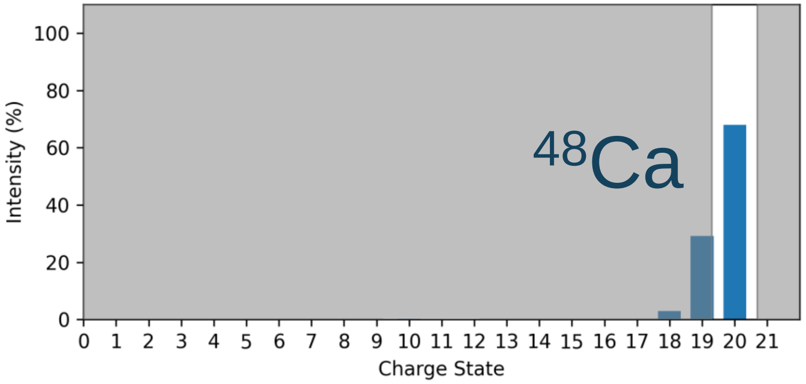

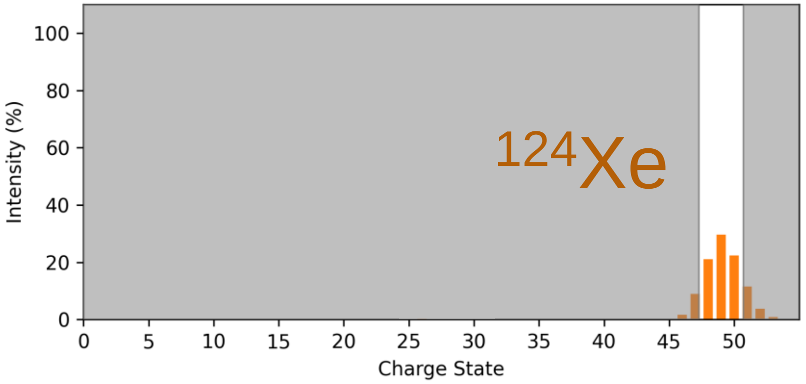

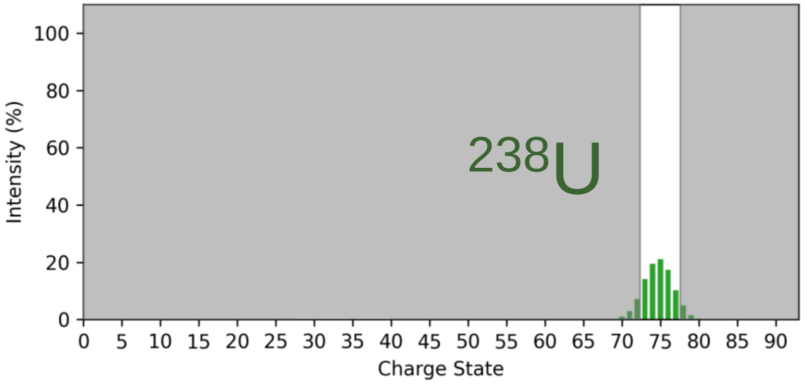

[1] Lapostolle, Septier, “Linear Accelerators”, 1970; [2] P.N. Ostroumov, et al., Phys. Rev. Lett. 86, 2798, 2001; [3] P.N. Ostroumov, et al., Phys. Rev. Lett. 126, 114801, 2021

Charge State Separation and Selection

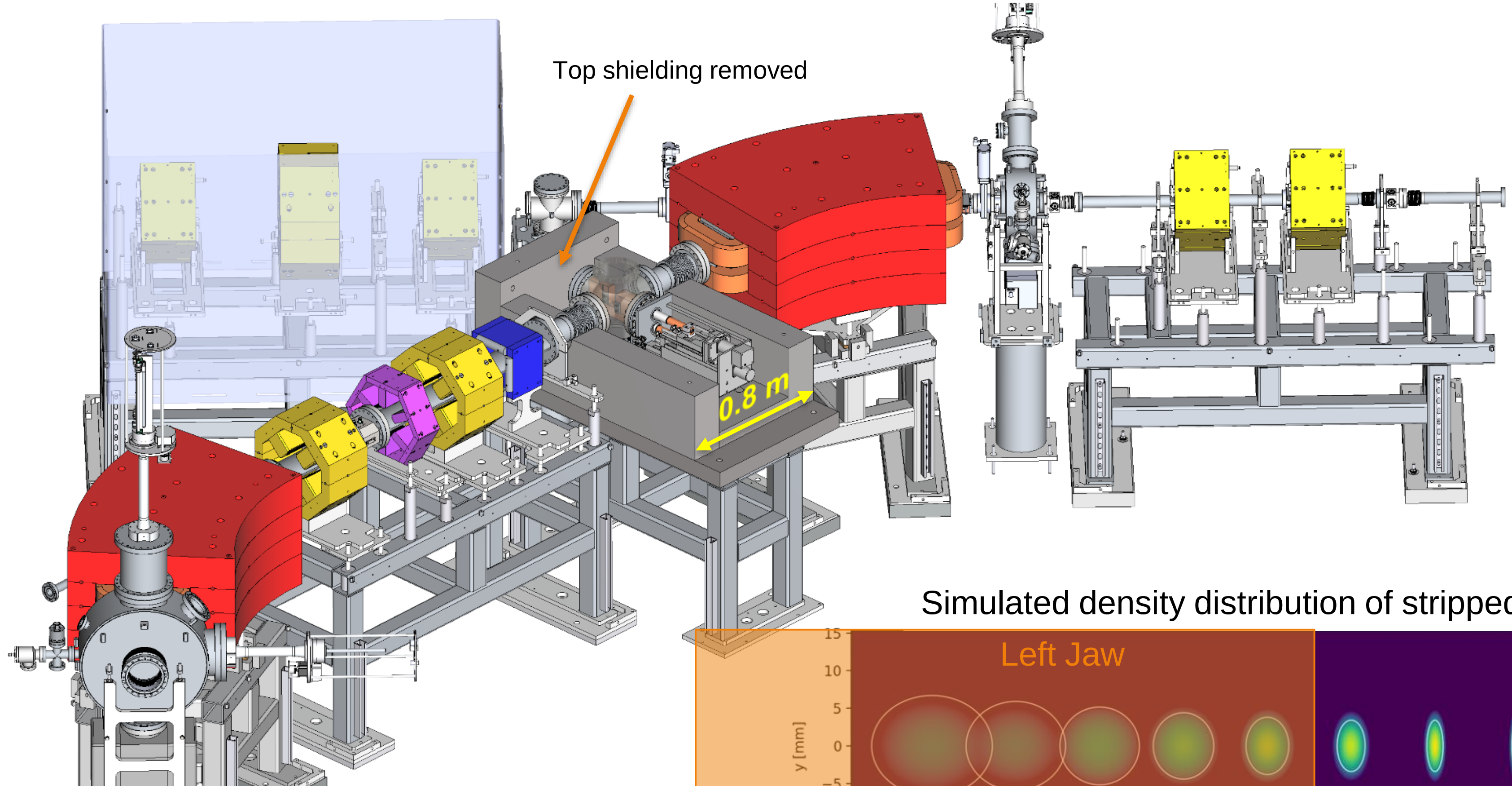

Beam from the Charge Stripper

- 180-deg achromatic and isochronous bend for transport of multi-charge-state beam

Simulated density distribution of stripped ^{238}U charge states (subject to changes)

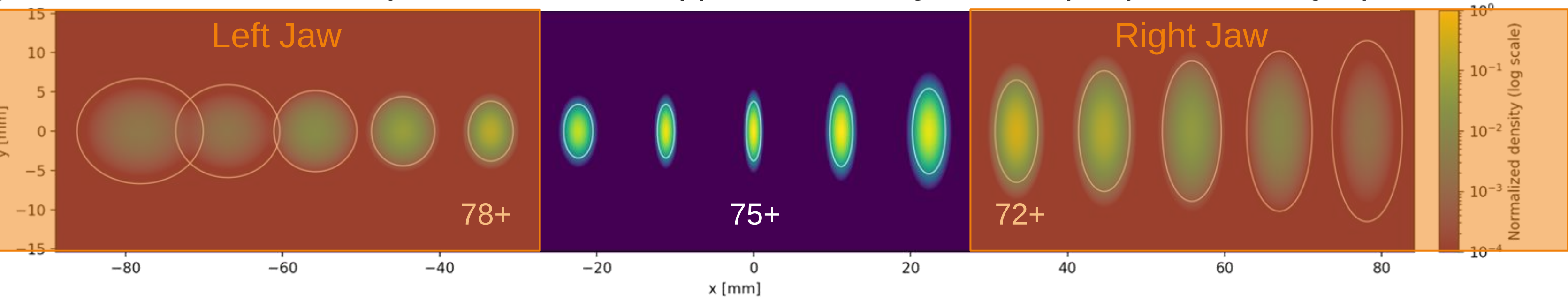

Low Power Charge Selector

- **Conventional** type of a **movable** beam collimator
  - Motion with 0.1 mm steps is necessary for precise positioning and scanning of the charge state distributions
- **Water-cooled** jaws
- Glidcop AL-15®
  (alumina dispersion-strengthened copper alloy)
- **500 W** per beam spot
  - Identified from initial thermal stress analysis
  - Designed to support **initial operations**
- In service since 2019 (since beam commissioning)
  - Including 4 years for user operations
    - 2019 – 2024: SN001, 437 kWh
    - 2024 – 2025: SN002, 355 kWh
    - 2025 – : SN003, 829+ kWh (still in use for another year)

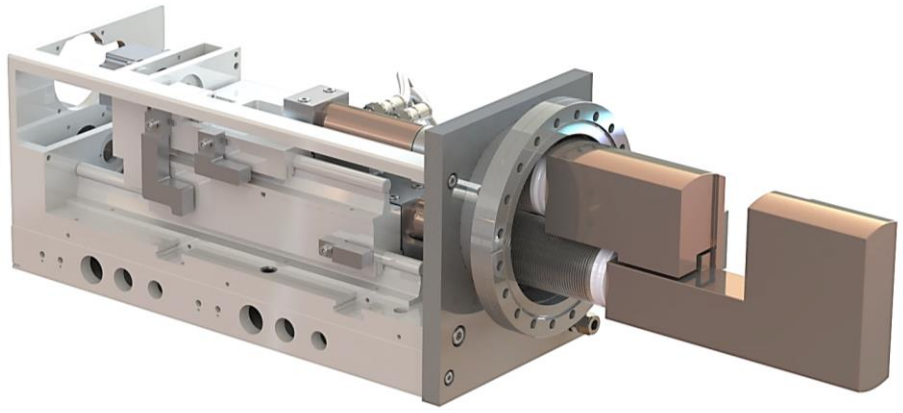

Charge Selector's Components Need Maintenance

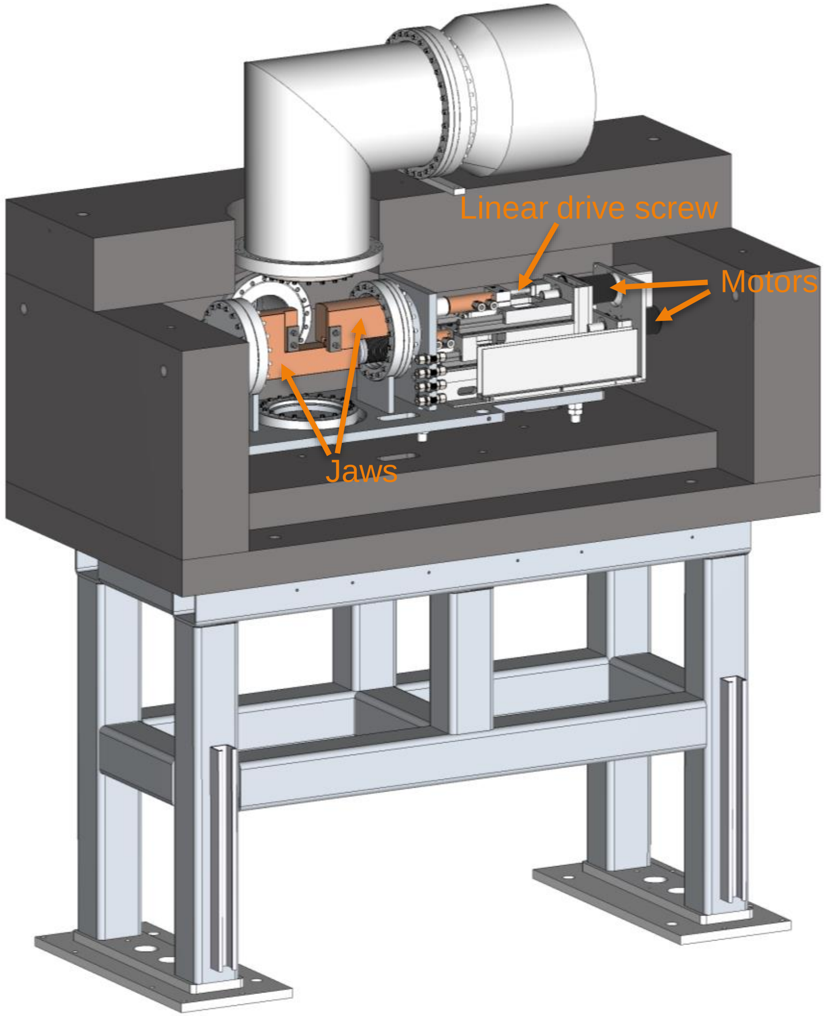

- Components that need periodic service
  - Drive screws, lubrication
  - Jaws, **inspection** and **replacement**
- Components that need service in case they fail
  - Motors and encoders
  - Limit switches

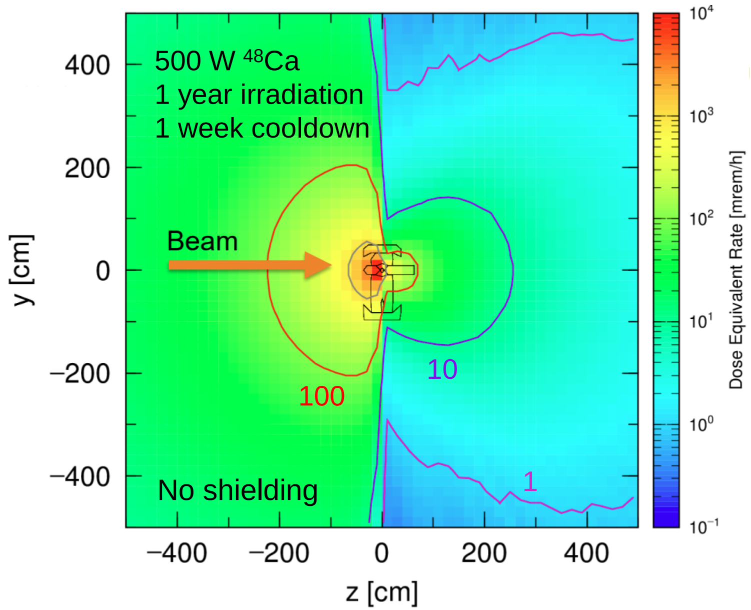

- Components are inside the shielding
  - Dose measured in Sep 2024 (2 months of cooldown after 10 kW operation): **800 mrem/h** (8 mSv/h) on contact
  - Reasonable agreement with calculated dose distribution
  - **Self-shielding** is significant

Maintenance Shielding

- We follow **common practices** for radiation work:
  - Shielding (workers stay preferably on the downstream side of the jaws, where self-shielding is effective)
  - Distance (use of remote tools, exclusion zone, etc.)
  - Time (planning of each maintenance operation)
- **Maintenance shielding** designed to achieve further reduction of the radiation dose to workers
  - Shielding block made of W-Cu can be installed even **before** the main **shielding is removed**, and can **stay** on the jaws when they are removed from the vacuum chamber
  - Allows for urgent repairs

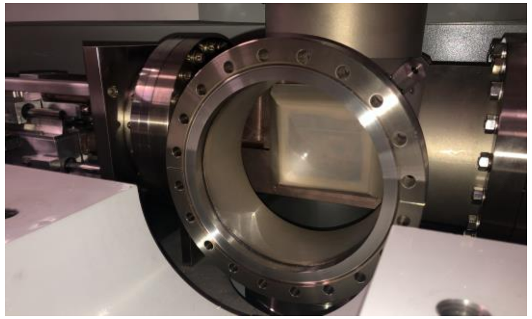

Top view

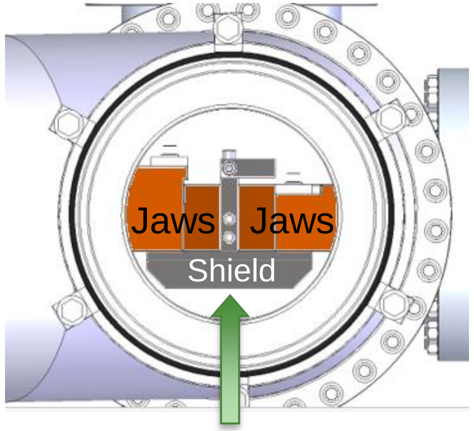

New port for the shielding block

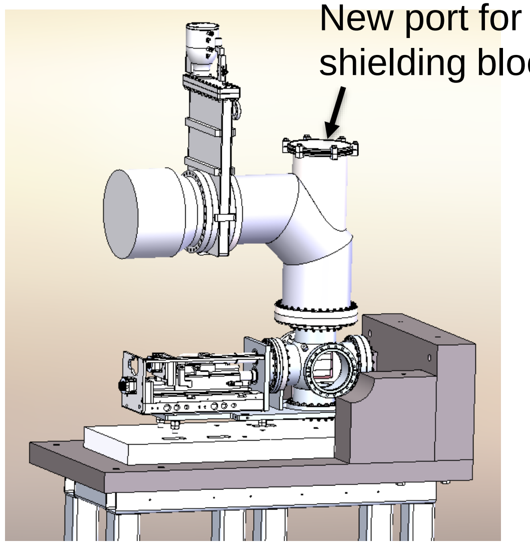

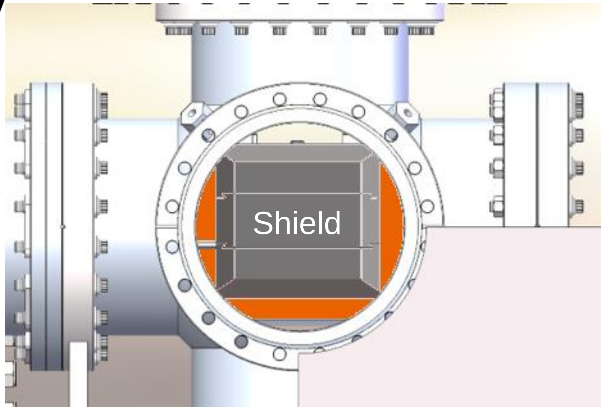

Front view

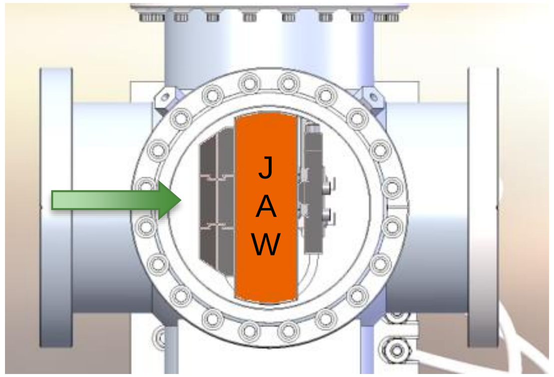

Side view

LPCS Supports Facility Operations with No Failures

- LPCS supported 1, 5, 10 and 20 kW operation of FRIB

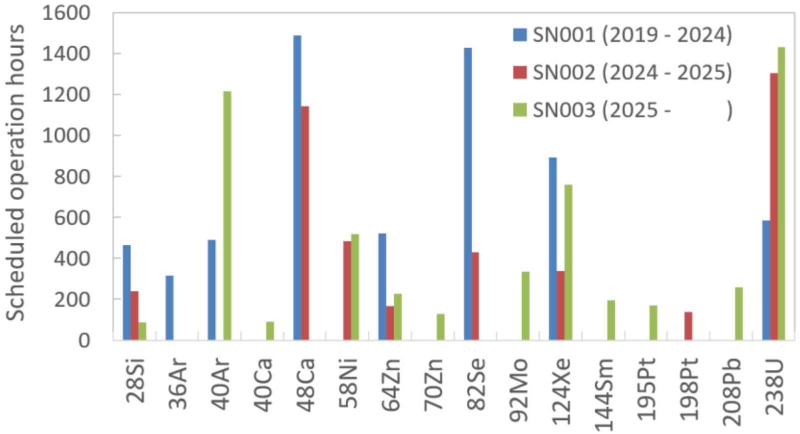

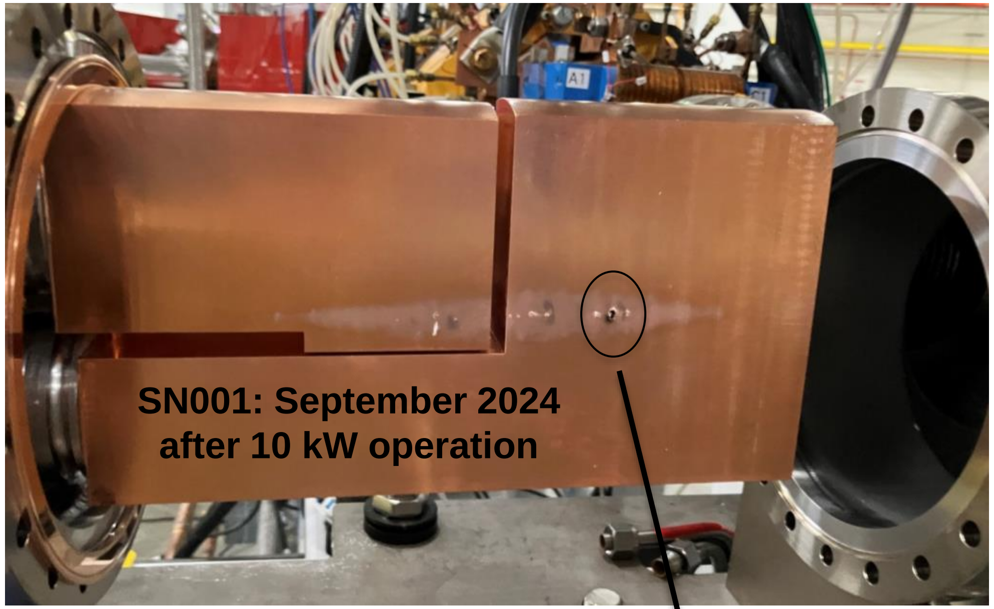

- SN001 jaws were inspected in September 2024
  - A noticeable “hole” was found on the outer jaw, ~ **1 mm** depth was measured later
  - Fluence at the spot $3 \cdot 10^{17}$ ions/mm^2, at $2 \cdot 10^{11}$ ions/mm^2/s

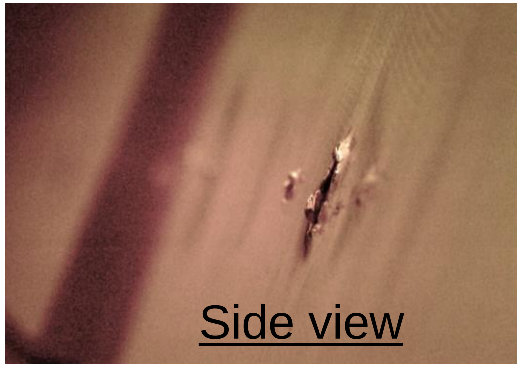

- Despite the **expected** surface damage, **no** major mechanical **issues** or any water **leaks** developed
- But what to expect in the future?

High Power Deposition

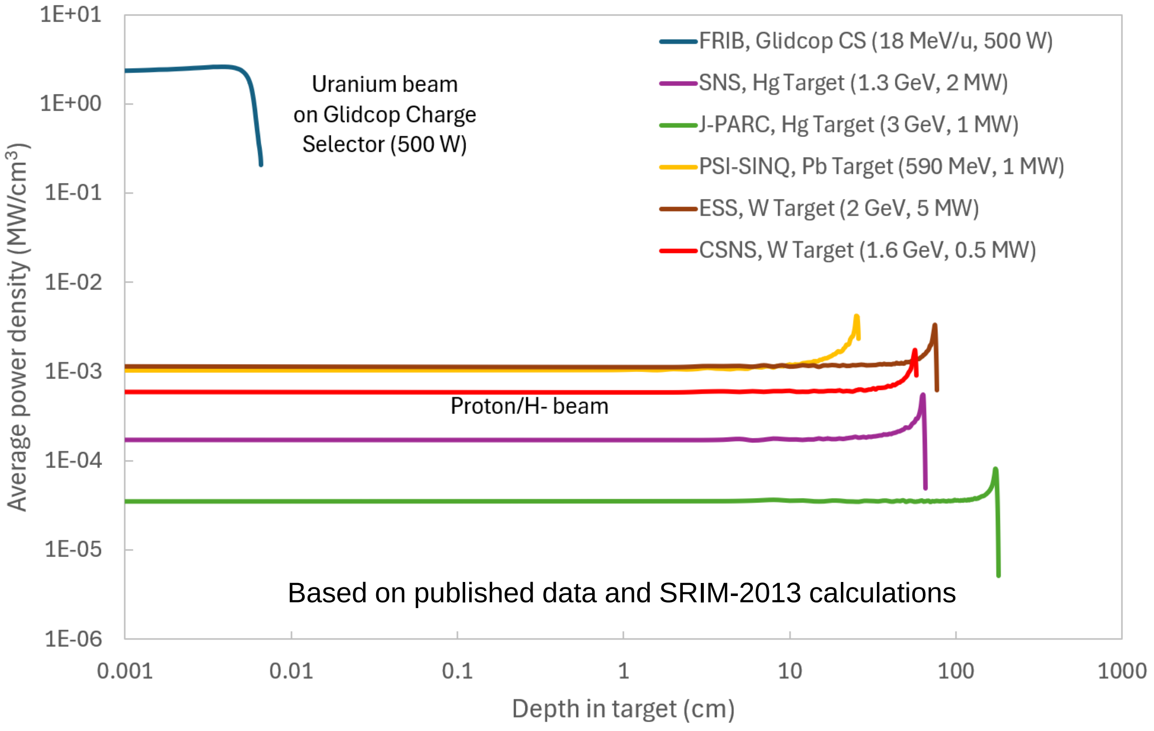

- Average power density deposited by FRIB heavy ion beams is orders of magnitude higher than produced by proton/H- beams in the highest power linear accelerators
  - Stopping power for **slow heavy ions** is much higher

$$\frac{dE}{dx} \sim \frac{Z^2}{\beta^2}$$

  - FRIB beams are focused into ~ **mm spot size** (requirement for charge state separation)
  - Spallation neutron sources, for example, do not require small beam spot on the target

Data sources:
M. A. Plum, M. Holding, and T. McManamy, “Beam Parameter Measurement and Control at the SNS Target”, in *Proc. PAC’05*
F. C. Pilat, “SNS Upgrade and Power Ramp Up”, presented at the HB’23
T. Wakui, et al. “Recent studies for structural integrity evaluation and defect inspection of J-PARC spallation neutron source target vessel”, Journal of Nuclear Materials, 506, 2018
F. Berg, et al., “Target studies for surface muon production”, Phys. Rev. Accel. Beams 19, 024701, 2016
H. D. Thomsen and S. P. Møller, “The Beam Delivery System of the European Spallation Source”, in Proc. HB’16
S. Fu and S. Wang, “Operation Status and Upgrade of CSNS”, in Proc. IPAC'19

Thermal Creep & Fatigue

- Heating causes material expansion and strain
- That induces thermal stress
- Maximum surface temperature of the Glidcop jaws should be **below** 678 K (**405**℃)
  - Above this temperature thermal creep must be considered
- We allow the material yield, i.e. plastic strain, allowing the **total strain** up to **0.35%**, to accept higher power load but avoid thermal fatigue after **5000** warmup-cooldown **cycles**

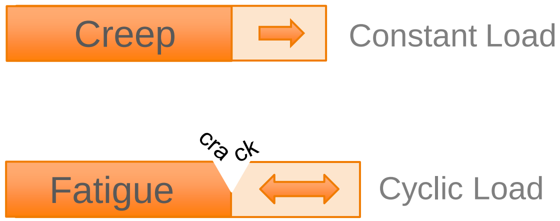

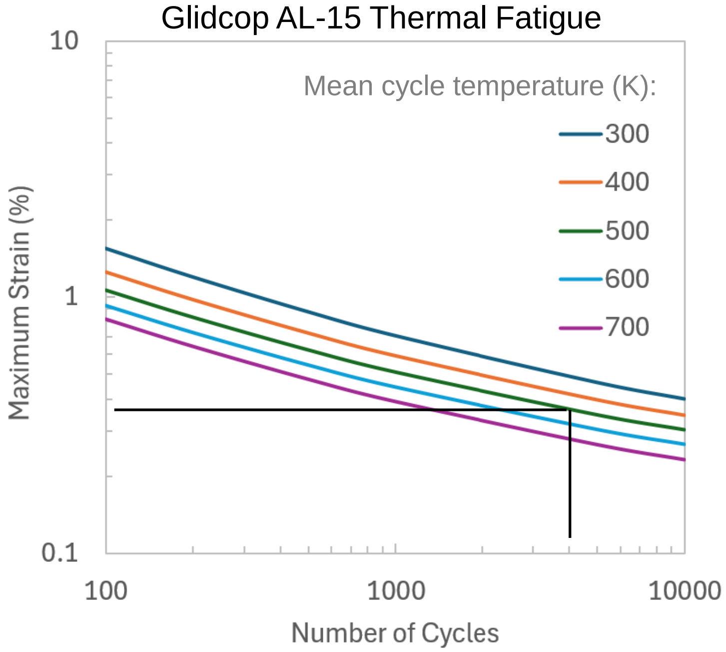

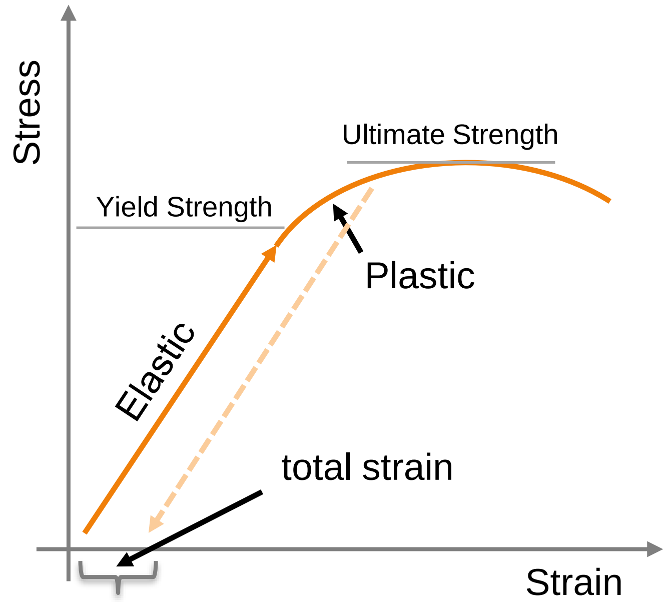

J. Collins et al. "Establishment of new design criteria for GlidCop X-ray absorbers". Journal of Synchrotron Radiation. 2017

Radiation Effects: Displacement of Atoms

- Radiation damage is a combination of detrimental effects. The primary source of the damage is displacements of atoms measured in **displacements per atom** or **dpa**. It is usually characterized by the **rate of dpa** in [DPA/s]
  - A DPA = 1.0 means that, on average, every single atom in a given volume of the material has been knocked out of its lattice site at least once
- Extremely high DPA rate due to heavy ions causes faster degradation of materials
  - Average DPA rate in Glidcop jaws is $5\cdot10^{-4}$ DPA/s @ 500 W
  - Over 1 week it builds up: **300** DPA
  - SNS 2 MW target, for example, has an administrative lifetime limit of **12** DPA [1]
  - Fusion reactor materials expect **10 – 20** DPA/year
  - Glidcop alloys exhibit good strength retention after irradiation, at least up to **150** DPA [2], although become softer at > 300℃

Glidcop irradiation, PHITS simulation

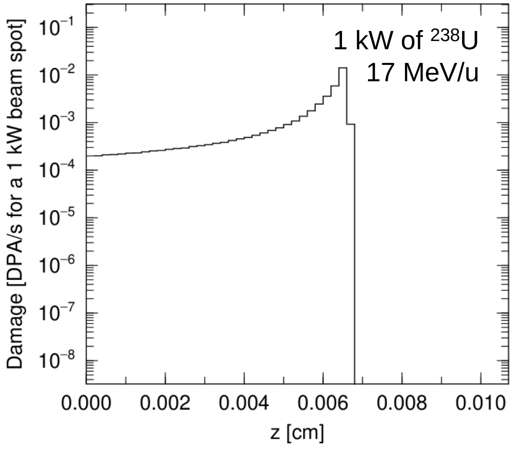

D.J. Edwards et al. / Oxide dispersion strengthened Cu alloys

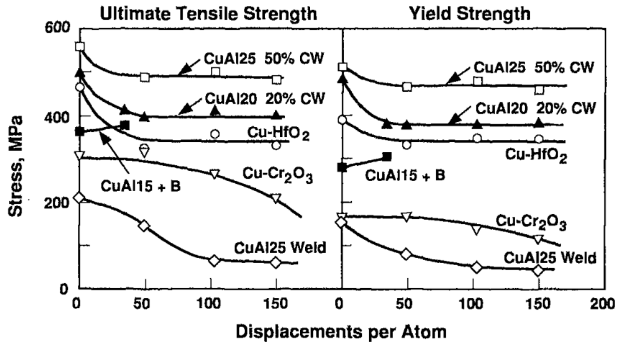

[2]

Fig. 3. Ultimate tensile and yield strength of GlidCop^{TM}, $Cu-Cr_2O_3$, and $Cu-HfO_2$.

[1] Johns, et al. Design and structural assessment of the Spallation Neutron Source 2.0 MW target, 10.1016/j.nima.2021.165799, 2021
[2] Edwards, et al. Irradiation performance of oxide dispersion strengthened copper alloys to 150 dpa at 415° C, Journal of Nuclear Materials, V. 191–194, 1992

Radiation Effects: Implantation

- Implantation of beam ions inside the absorber material
  - Result in **200% atomic** ratio, after 200 kWh ($5 \cdot 10^{18}$ ions of ^{48}Ca in SN001)
- Formation of alloys with **lower melting** temperature

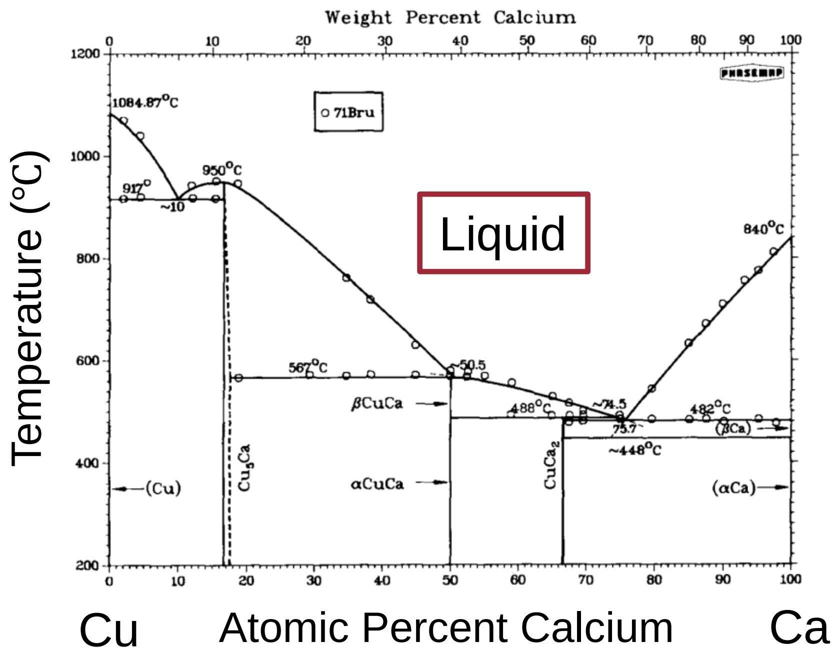

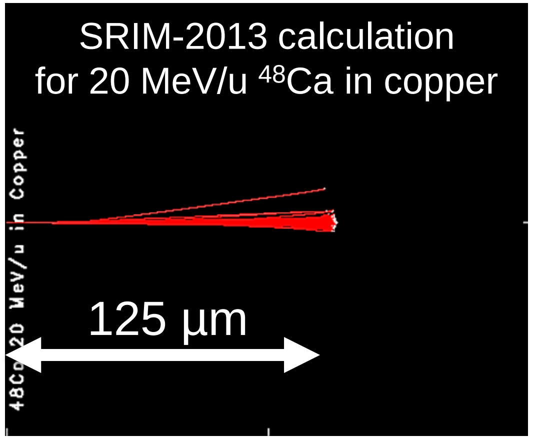

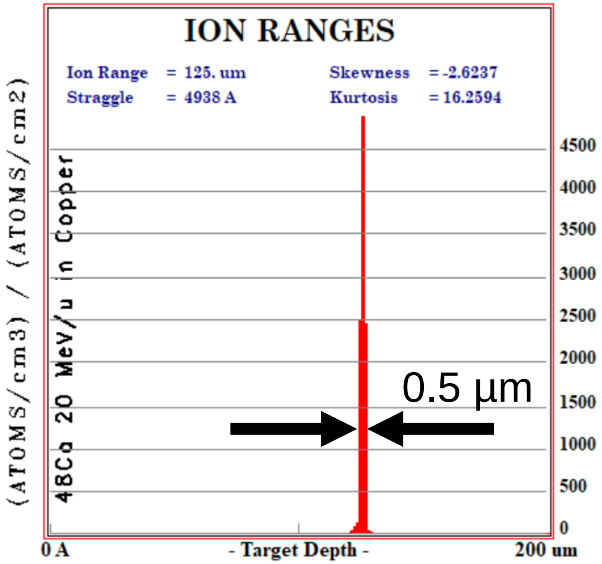

[Chakrabarti, D.J., Laughlin, D.E. The Ca−Cu (Calcium-Copper) system. *Bulletin of Alloy Phase Diagrams* **5**, 570–576 (1984)]

Radiation Effects: Swelling & Activation

- Accumulation of hydrogen and helium
  - About **0.1%** of the intercepted beam ions collide with copper atoms
  - **Protons, neutrons, and α-particles** are byproducts of these collision
  - Protons and α-particles stop in the material, capture electrons and become **hydrogen** and **helium** atoms
  - These atoms tend to agglomerate producing **voids** and **gas bubbles** inside the material causing **swelling**, and **blistering** on its surface

  [Was, Fundamentals of radiation materials science, Springer, 2007]

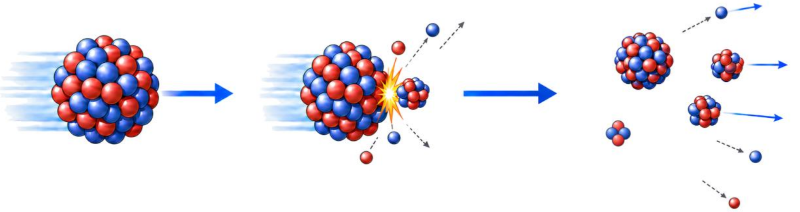

- Isotope Production and Radioactivation
  - Most nuclear reaction products are **radioactive nuclei**
  - Neutrons **activate** the jaws, assembly parts, shielding, etc.
  - β decay (**γ-ray emission** accompanying it) of these isotopes and nuclei of activated materials is the main source of **residual radioactivity**
- **Prompt** radiation elevates the background level of the radiation loss monitors, making them **less sensitive** to small beam loss

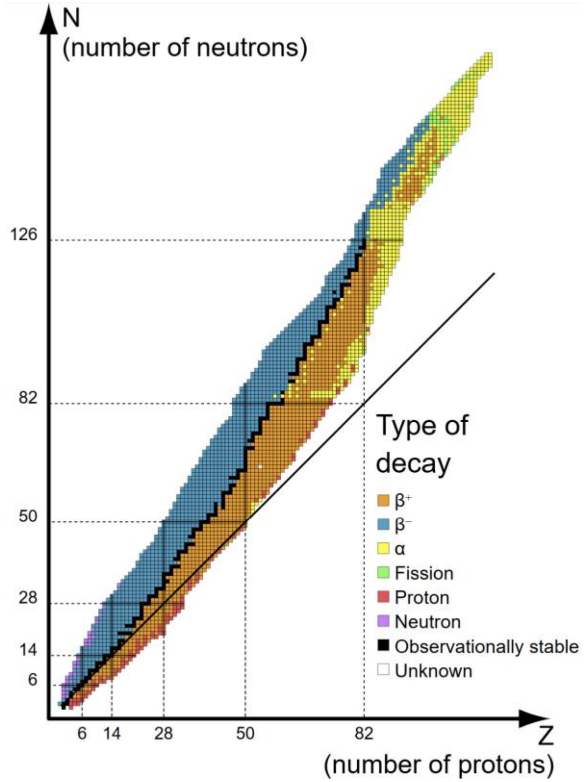

[https://commons.wikimedia.org/wiki/File:Table_of_nuclides_(mul).svg]

Improvement: Multiple-Charge-State Acceleration

- ^{48}Ca beam brings the most radioactivity to the jaws "per watt".
- **Two-charge-state** ^{48}Ca tune was developed and successfully applied since October 2024.
  - This is challenging, $\Delta Q/Q = \pm 0.5/19.5 = \pm 2.6\%$ as wide as that of **5Q** uranium $\pm 2/75 = \pm 2.7\%$, but does **not** have a central "**reference**" charge state.
  - Stripping efficiency improved from **68%** to **97%**, by factor of 1.43.
  - Load on the charge selector jaws reduced to 90 W @ 20 kW on target
- Minimizes **power** of unwanted charge states
- Minimizes the **activation** of the machine
- Minimizes the radiation **background** level for loss detection
- Saves precious beam **intensity**

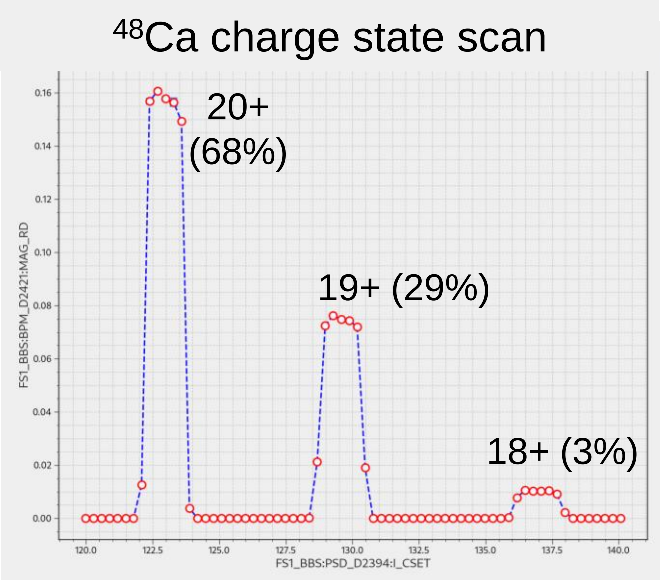

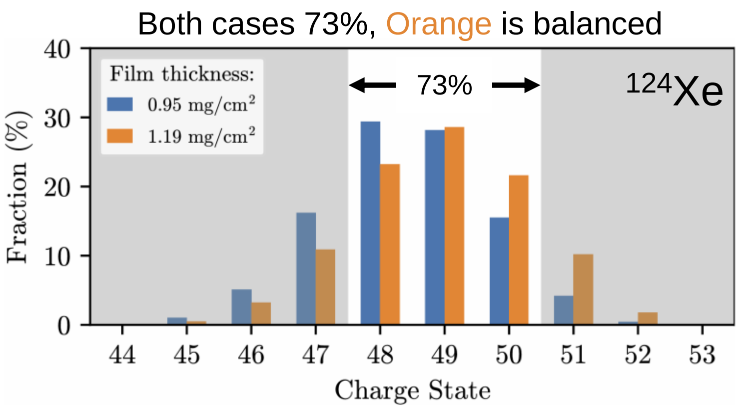

Improvement: Increase Angle of Incidence

- Titled jaw surface allows **1640** W compared **500** W in the original design
  - Radiation damage is also distributed over larger area and closer to the surface
- This charge selector modification will be used starting **2027**

Overhang is still necessary for self-shielding

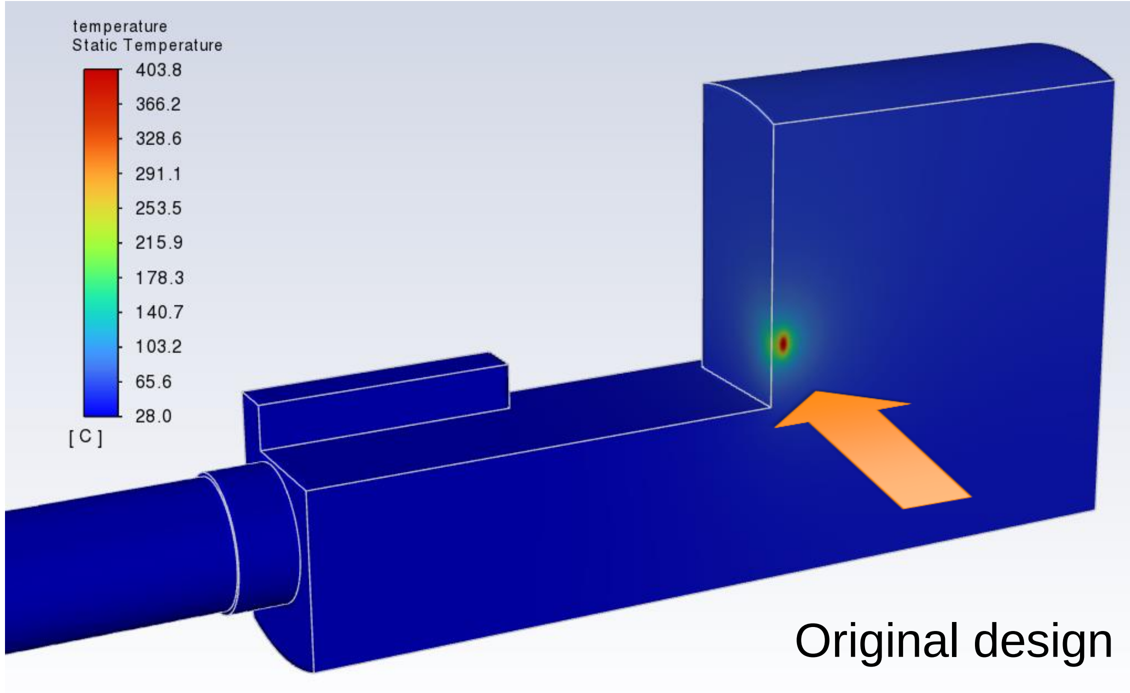

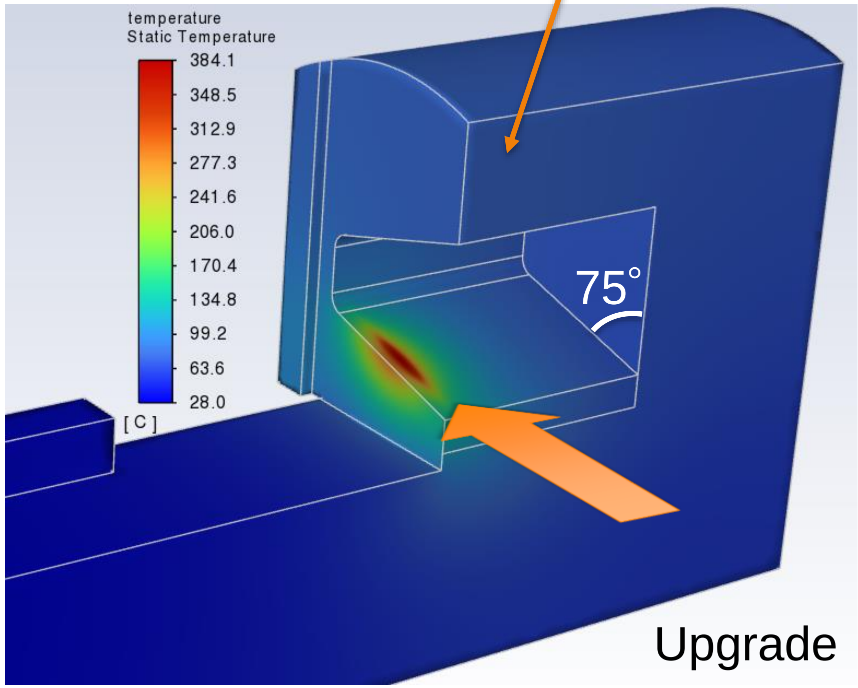

Heat Transfer by Thermal Radiation

- The new charge selector shall support much higher power, up to **5 kW per spot**, 8 kW per jaw
  - High power load requires highly efficient heat transfer
  - Radiation provides heat transfer “at the speed of light”, but efficient only at high temperature

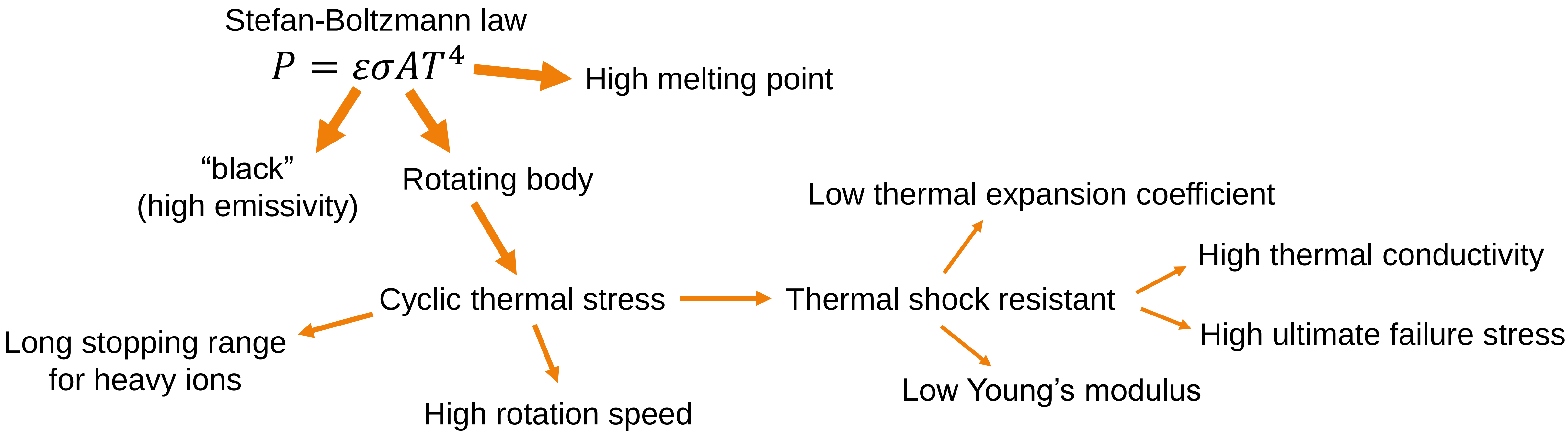

Thermal Shock Resistance

- 5 kW on the surface of **stationary** Glidcop and Graphite blocks, at 75 deg incidence
  - Glidcop: **convectively-cooled** back surface (10,000 W/m^2/K)
  - Graphite: **radiative** heat transfer from the front surface (ε = 0.8)

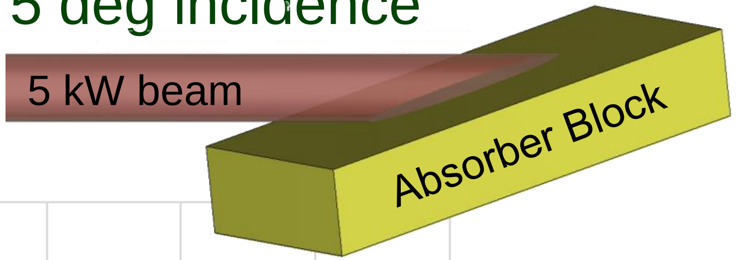

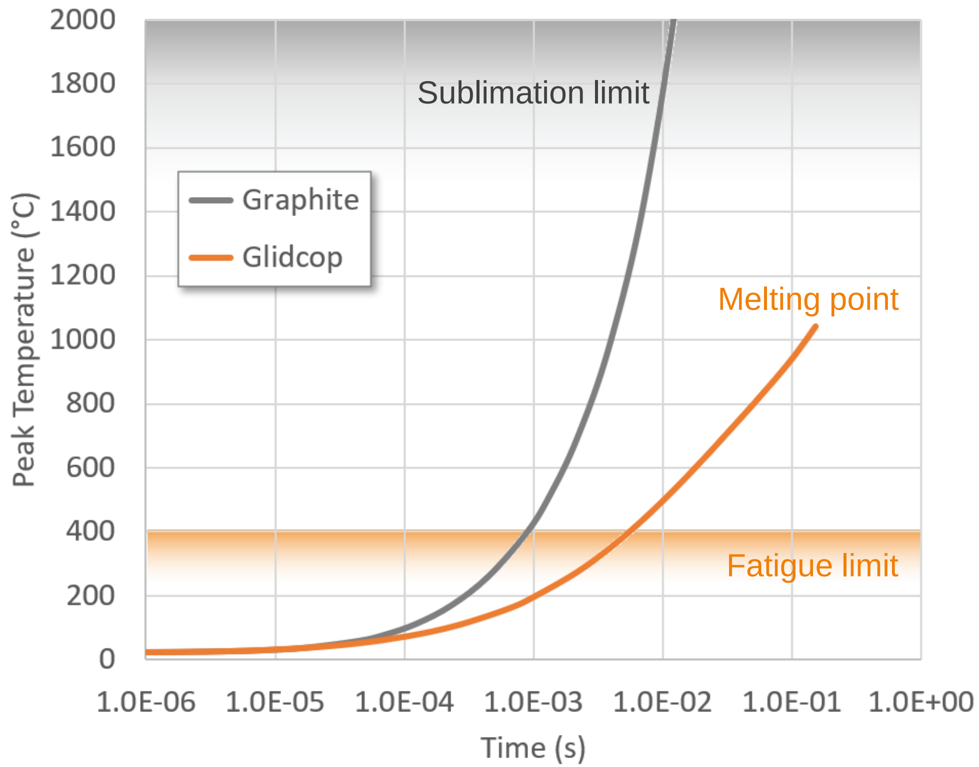

10 ms for graphite, 5 ms for Glidcop

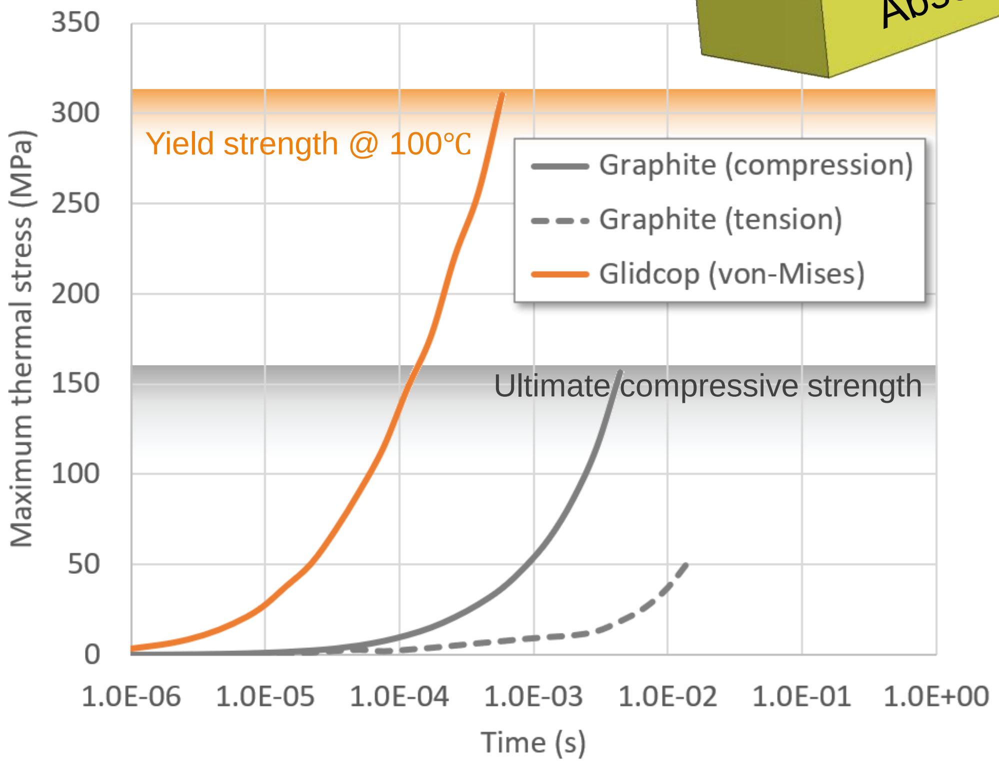

5 ms for graphite, **only 0.5 ms for Glidcop**

Advanced Charge Selector Concept

- Rotating graphite wheel (4’’ ≈ 100 mm diameter)
  - **Size** defines the **mean** temperature
  - **Rotation** speed defines **peak** temperature and **cyclic** thermal stress

$$\frac{P}{A} \sim T^4$$

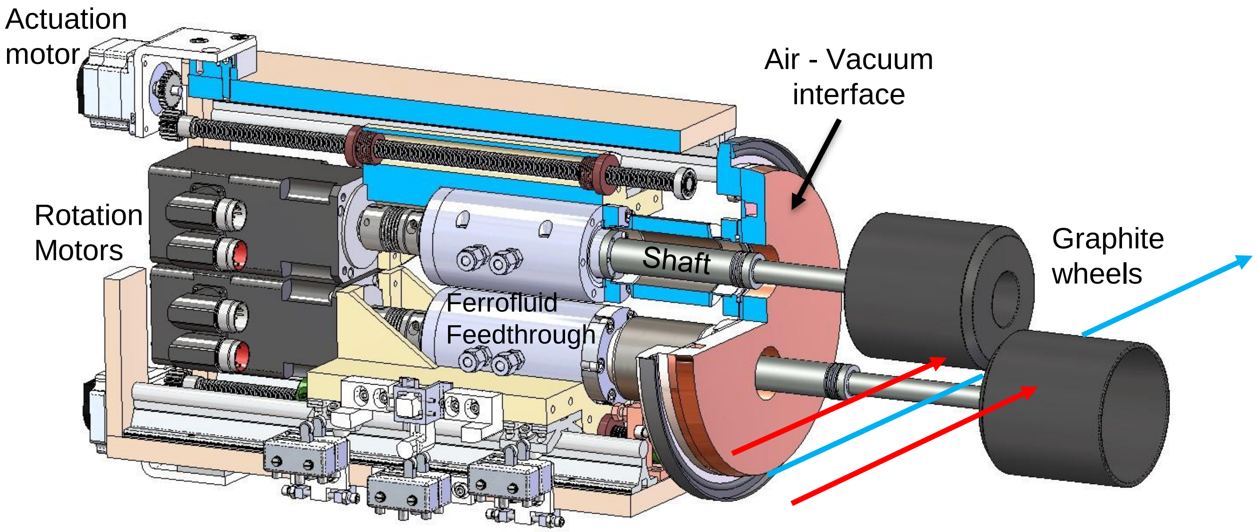

Vertically stacked graphite wheels to fit into available space

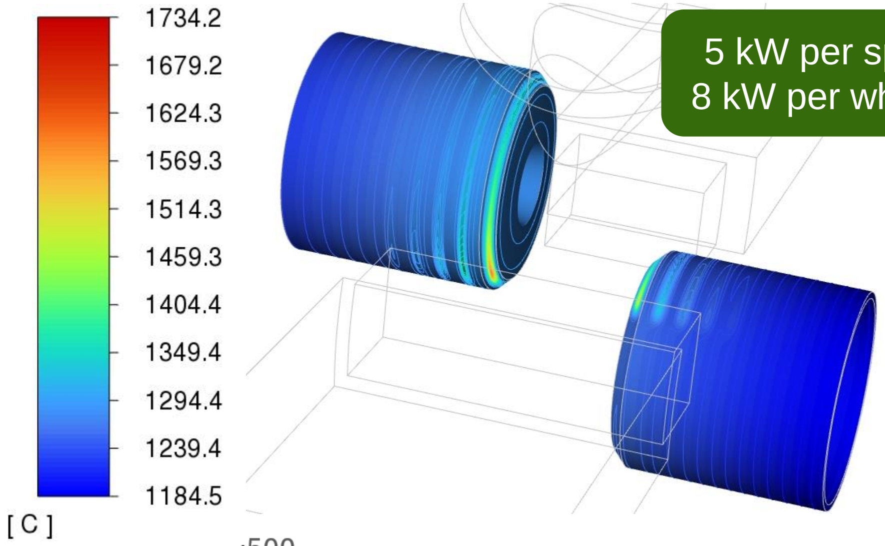

5 kW per spot
8 kW per wheel

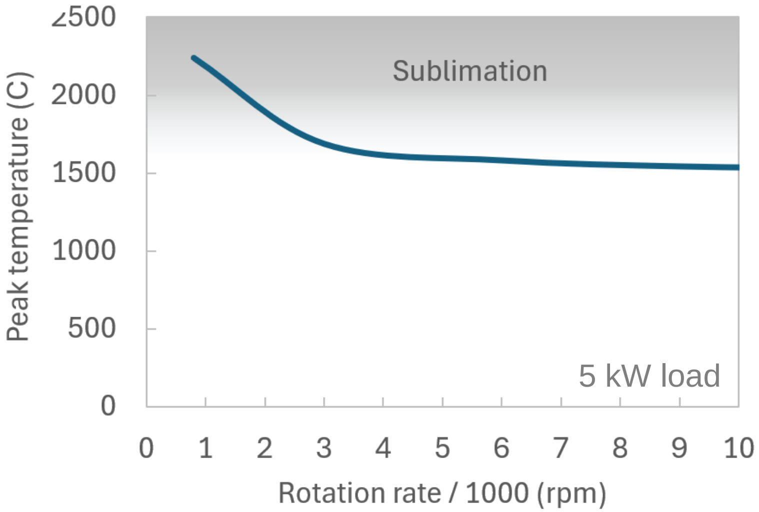

[A. Plastun et al., "Advanced charge selector for stripped heavy ion beams", in Proc. IPAC'24]

Power Density Comparison

- Instantaneous power density in the charge selector wheel (5 kW per ^{238}U spot) is **comparable** with that in the graphite target with **16 kW** 193 MeV/u ^{238}U beam

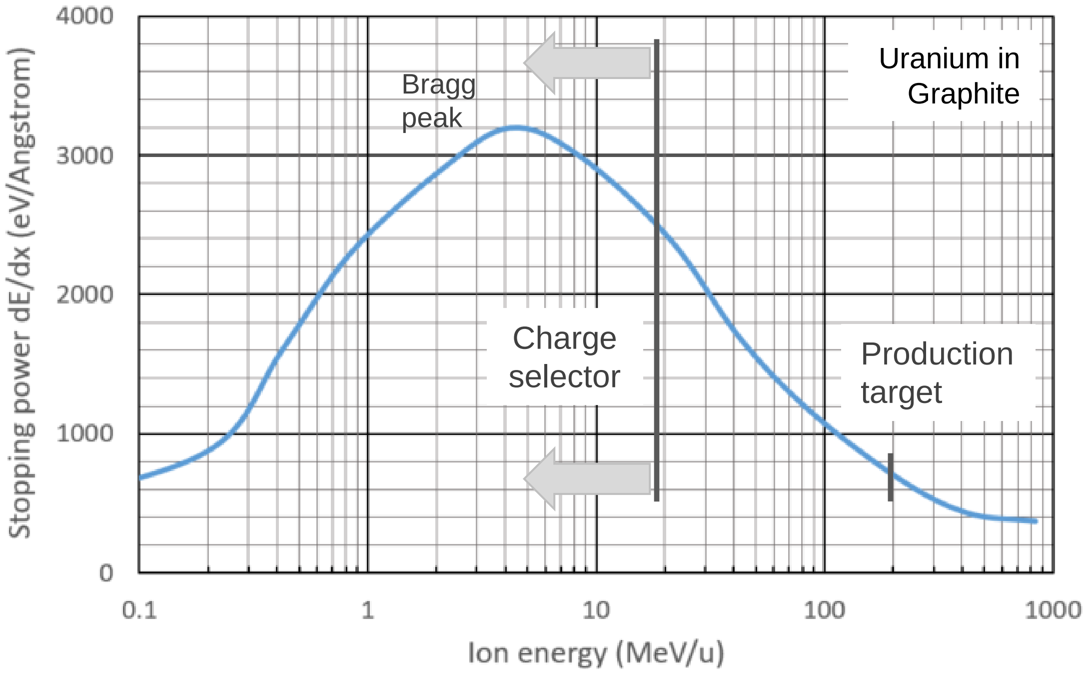

	Target	Charge Selector	
Beam energy	193	16.5	MeV/u
Deposited power	**5.0**	**5.0**	kW
Stopping range	(disk thickness) 2.1	0.15	mm
Spot size	0.25 x 0.25	0.70 x 1.25	mm
Instantaneous density	**6.0**	**6.0**	kW/mm^3
Averaged over circumference	0.004	0.06	kW/mm^3
Linear spot velocity	8 (500 RPM)	32 (6000 RPM)	m/s

FRIB Target
30 cm diameter
500 RPM

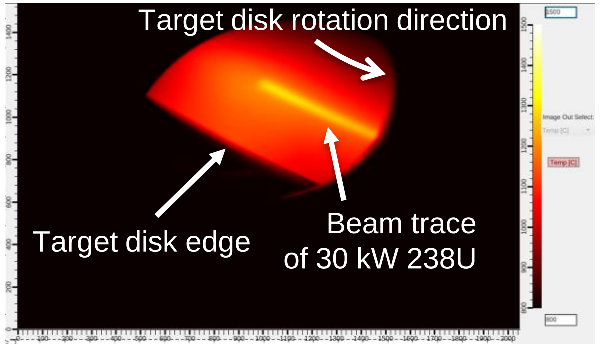

Fatigue-Resistant Shaft Material

- The shaft must:
  - withstand the graphite temperature at the hub (1000-1200℃)
  - withstand cyclic cantilever load

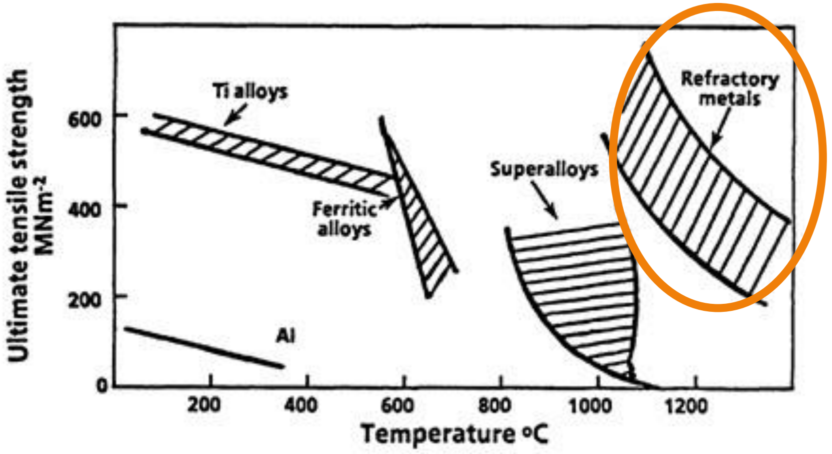

- Refractory metals: Nb, Mo, W, Ta, Re
- TZM Alloy (~99% Mo, 0.5% Ti, 0.08% Zr, and 0.02%C)
  - Melting Point: 2,623℃

Notched fatigue test for TZM and TZC

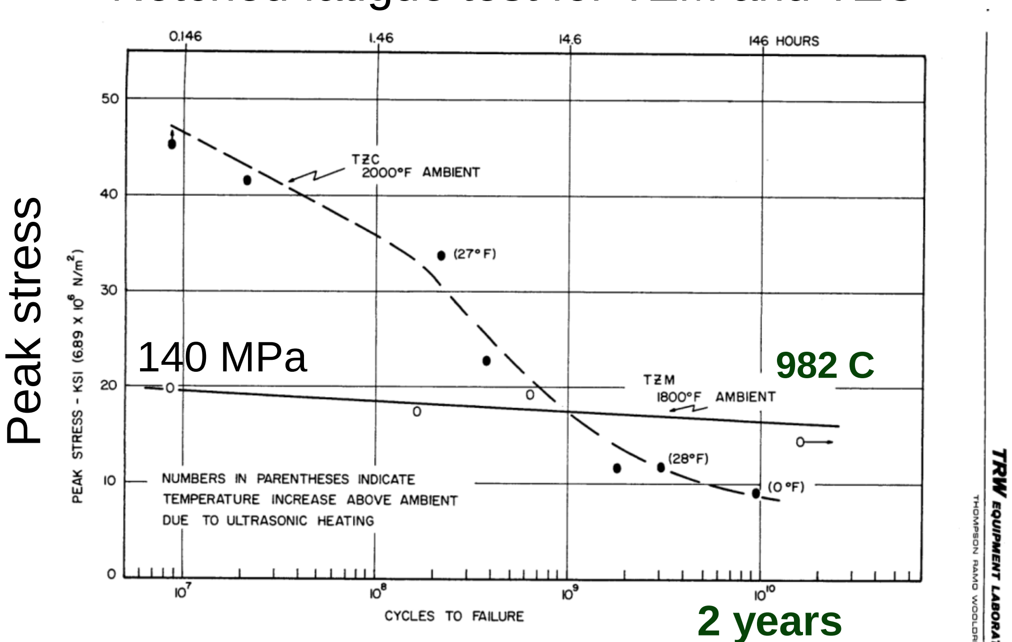

FIG. 6: FATIGUE CURVES FOR TZM (RECRYSTALLIZED AT 3092°F) AND TZM (STRESS-RELIEVED CONDITION) TESTED IN VACUUM ENVIRONMENT <10^{-8} TORR.

[Determination of elevated-temperature fatigue data on refractory alloys in ultra-high vacuum, CR 54775, Prepared for: NASA, October 15, 1965]

Thermal Expansion Management

- Hub and wheel made of different materials, **expand differently** when heated, particularly during transients
- To **avoid over-constraining** brittle graphite, the hub maintains constant load while keeping the wheel centered
  - Spring at the **lower temperature** side (~ 200℃ - 300℃)
  - Spring force is transferred via the tube surrounding the shaft (shaft sleeve) to the hub
  - **Force** is almost **constant** because the differential thermal expansion is in sub-mm range
  - Conical hub holds the **wheel aligned** no matter what are their temperatures

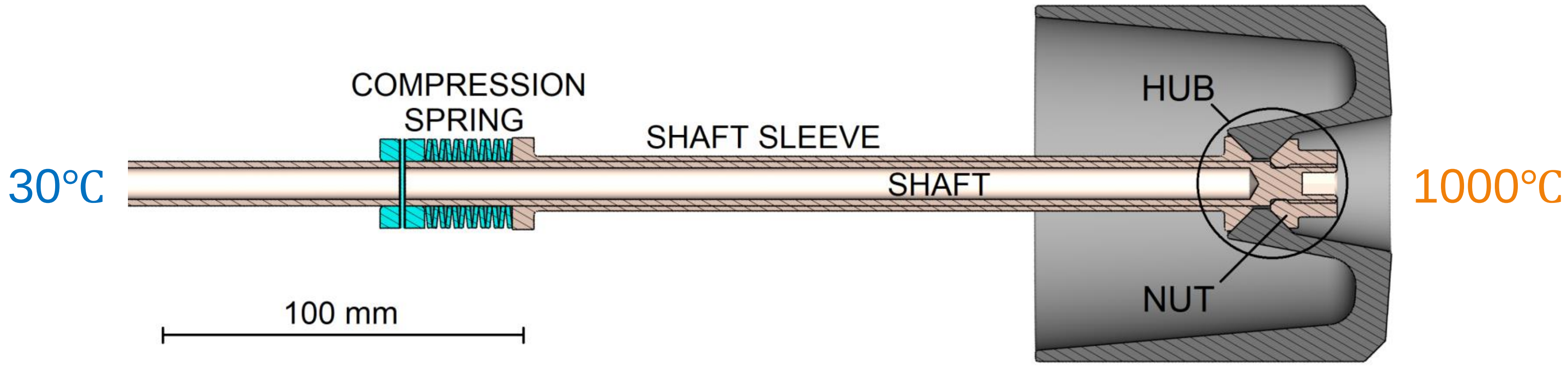

Vibration Test

- Pendulum mode of the shaft and the wheel assembly is 32.2 Hz
  - 32.2 Hz = 1930 RPM, below the region of interest (above 4,000)
  - Rotation must be **supercritical**, i.e. system must pass through a few resonances
- A vibration testbench was built to observe the system's behavior
  - After quickly passing two resonances (static pendulum mode gets transformed into forward and backward whirl modes) the wheel **rotation is stable** between 4,000 and 10,000 RPM (tested for one hour)

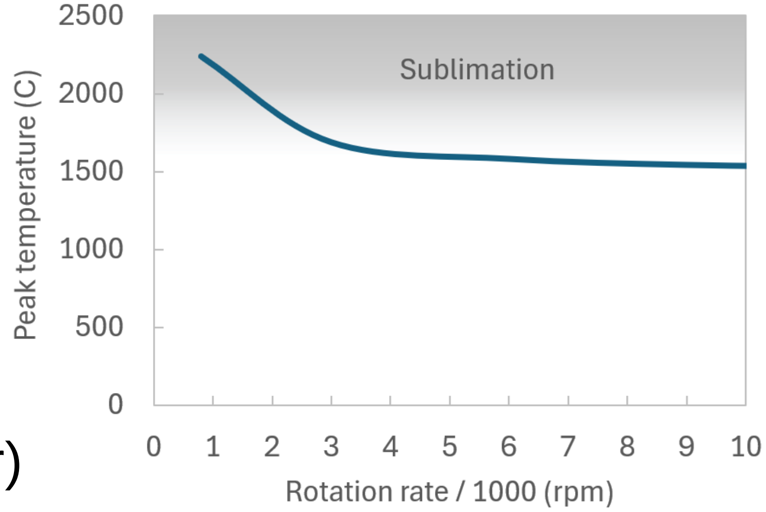

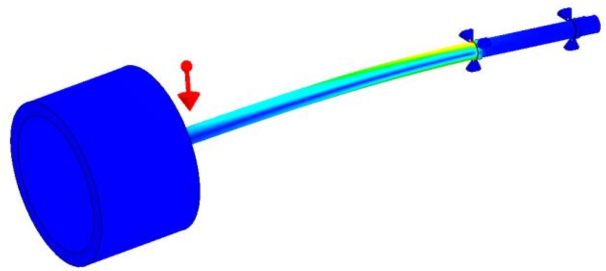

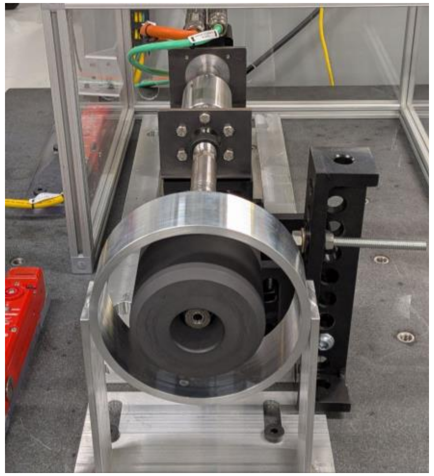

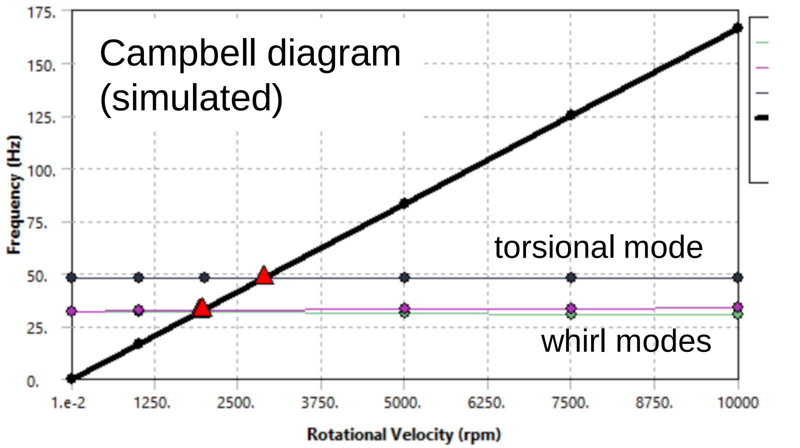

Radiation Damage Annealing

- Rotational design distributes radiation damage over larger area
  - » By a factor of 100, compared to static jaws

PHITS simulation, ^{238}U at 200 MeV/u

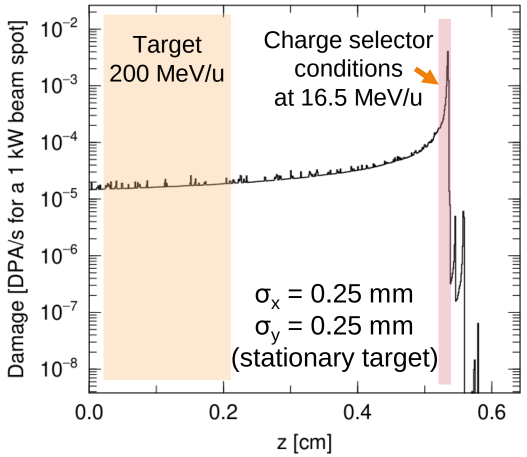

Rotating charge selector
at 5 kW: **40** DPA/week

Rotating Ø30-cm target disk
at 20 kW: **0.14** DPA/week

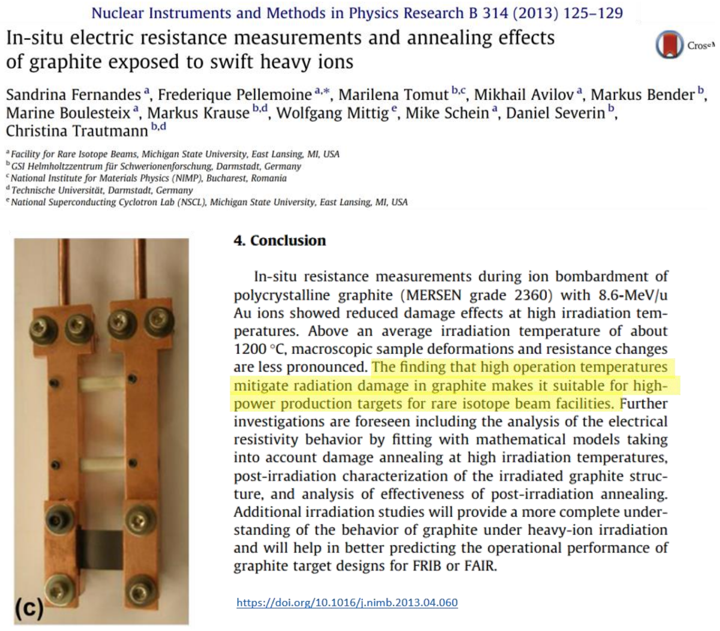
Nuclear Instruments and Methods in Physics Research B 314 (2013) 125–129

In-situ electric resistance measurements and annealing effects of graphite exposed to swift heavy ions

Sandrina Fernandes[a], Frederique Pellemoine[a,*], Marilena Tomut[b,c], Mikhail Avilov[a], Markus Bender[b], Marine Boulesteix[a], Markus Krause[b,d], Wolfgang Mittig[e], Mike Schein[a], Daniel Severin[b], Christina Trautmann[b,d]

[a] Facility for Rare Isotope Beams, Michigan State University, East Lansing, MI, USA
[b] GSI Helmholtzzentrum für Schwerionenforschung, Darmstadt, Germany
[c] National Institute for Materials Physics (NIMP), Bucharest, Romania
[d] Technische Universität, Darmstadt, Germany
[e] National Superconducting Cyclotron Lab (NSCL), Michigan State University, East Lansing, MI, USA

(c)

4. Conclusion

In-situ resistance measurements during ion bombardment of polycrystalline graphite (MERSEN grade 2360) with 8.6-MeV/u Au ions showed reduced damage effects at high irradiation temperatures. Above an average irradiation temperature of about 1200 °C, macroscopic sample deformations and resistance changes are less pronounced. The finding that high operation temperatures mitigate radiation damage in graphite makes it suitable for high-power production targets for rare isotope beam facilities. Further investigations are foreseen including the analysis of the electrical resistivity behavior by fitting with mathematical models taking into account damage annealing at high irradiation temperatures, post-irradiation characterization of the irradiated graphite structure, and analysis of effectiveness of post-irradiation annealing. Additional irradiation studies will provide a more complete understanding of the behavior of graphite under heavy-ion irradiation and will help in better predicting the operational performance of graphite target designs for FRIB or FAIR.

https://doi.org/10.1016/j.nimb.2013.04.060

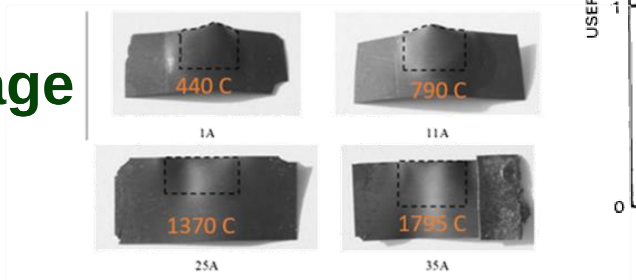

Fig. 4. Photos from all irradiated graphite samples after removal from holder. Irradiated areas are marked by black dashed rectangles.

Neutron irradiation data

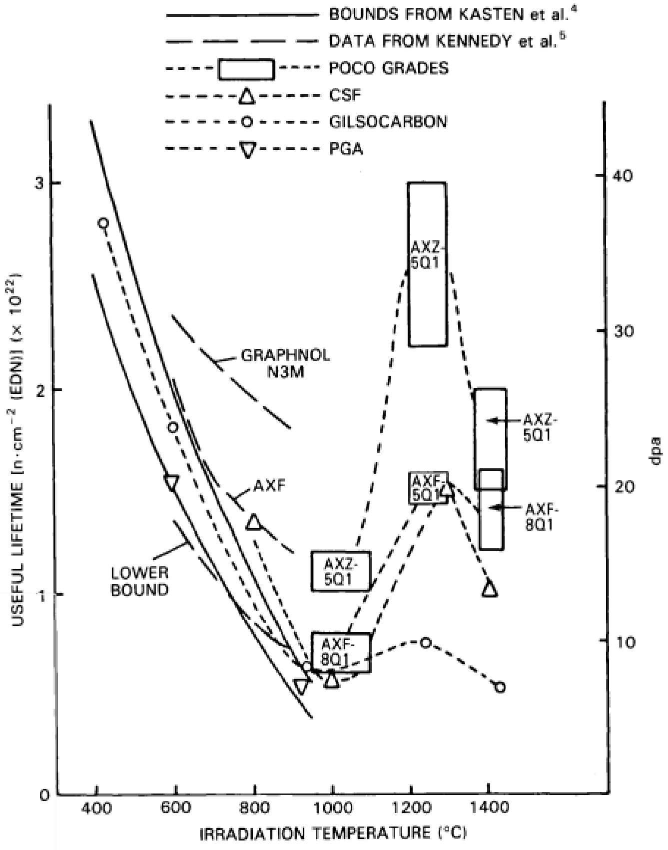

Fig. 11. Useful lifetimes.

[Kelly, B.T., 1989. Irradiation behavior of fine-grain graphites. Fusion Technol. 16, 96–103.]

- Graphite supports **annealing of radiation damage**
  - At above 1200℃, observed on small foil samples
- Graphite supports diffusion of implanted ions
  - Graphite is porous
  - High temperature **enhances diffusion** $D = D_0 e^{-\frac{E_A}{RT}}$

Activity & Residual Radiation

- Although activity and radiation damage are distributed by larger area, the total amount of **activity increases with beam power**
- Activity and residual dose rate **saturate** over a few weeks
- Main source of the residual radiation is graphite (**1** R/h or **10** mSv/h, @ 30 cm)

Simulated with 1 kW of ^{48}Ca

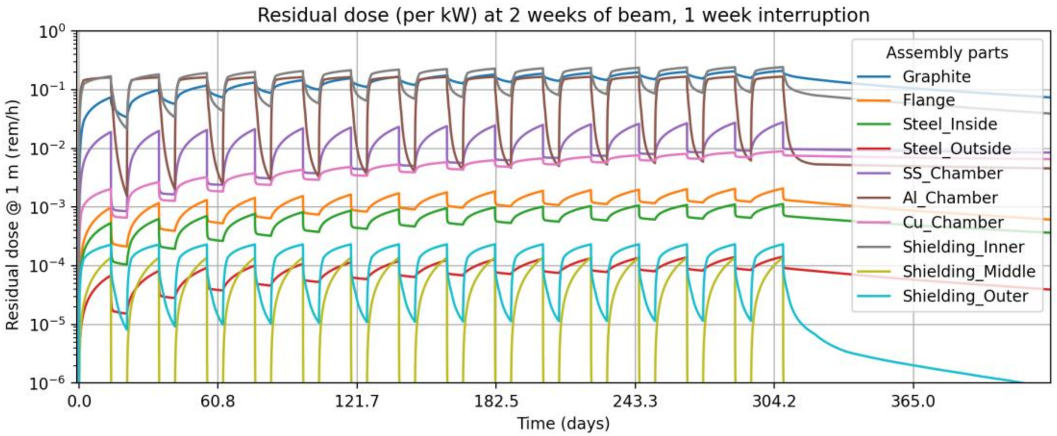

Residual dose rate distribution after 1 kW of ^{48}Ca
(1-year continuous beam exposure, 1 hour cooldown)

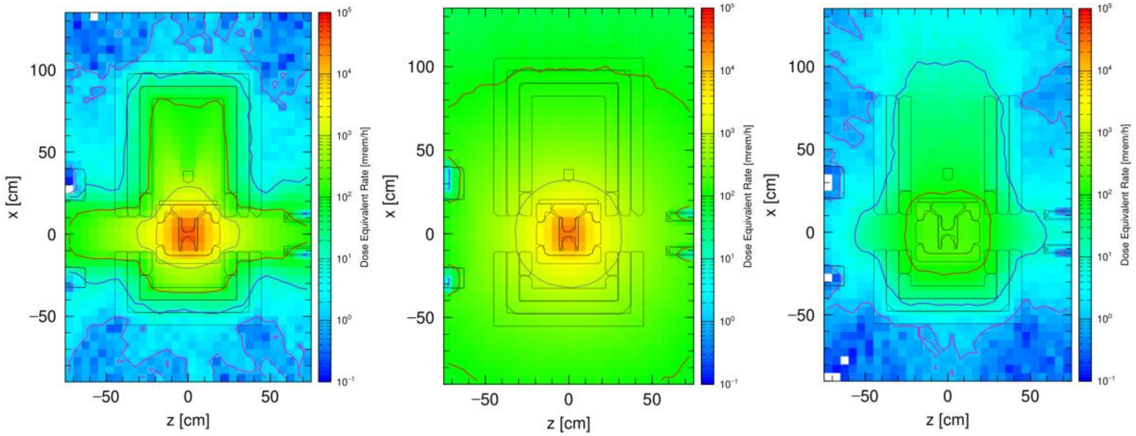

Whole assembly with shielding | Graphite only, no shielding | Assembly w/o graphite

- No self-shielding effect for graphite jaws

Maintenance & Remote Handling

- The primary maintenance task is replacement of the graphite wheels
  - Periodicity would depend on the graphite lifetime, which is difficult to predict. It must survive at least a single experiment, i.e. about **1 week**.
  - Today, shielding can only be removed using a mobile crane (no overhead crane in the linac tunnel), which is not practical for weekly or even bi-weekly maintenance operations. Doors with **actuators** solve this problem.
  - Activated graphite wheels require **remote handling**.

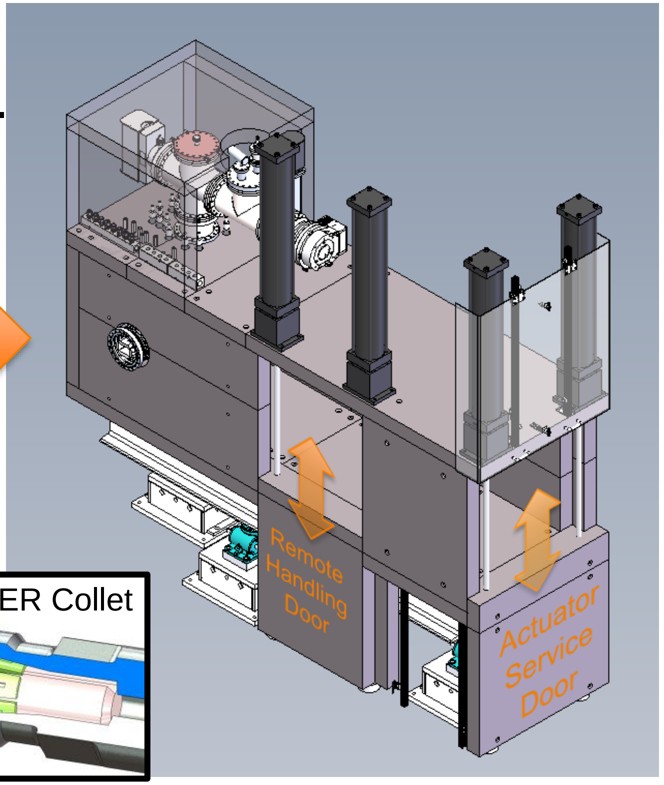

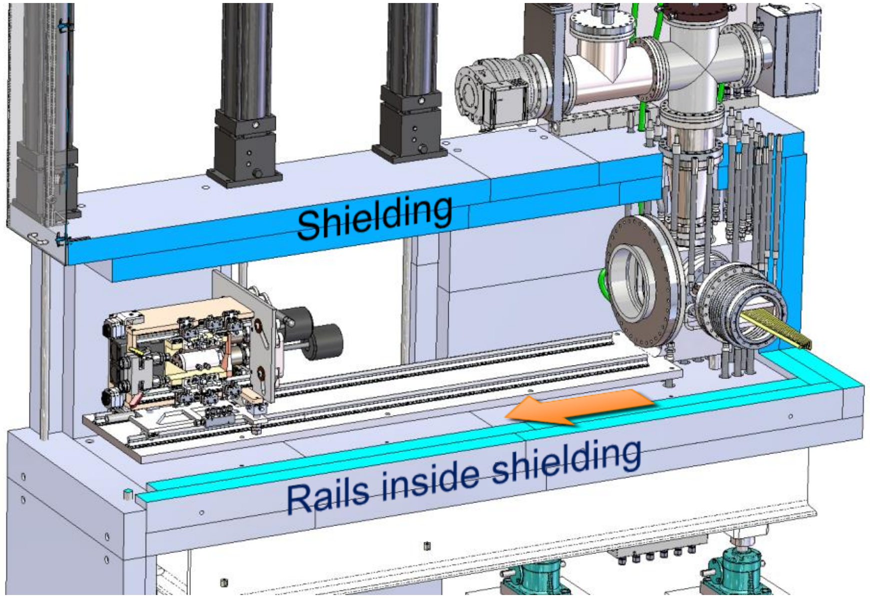

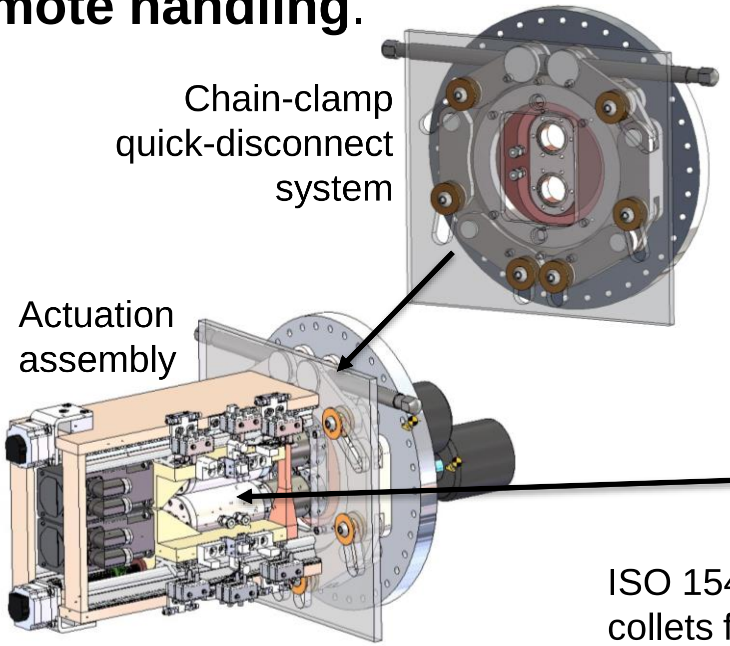

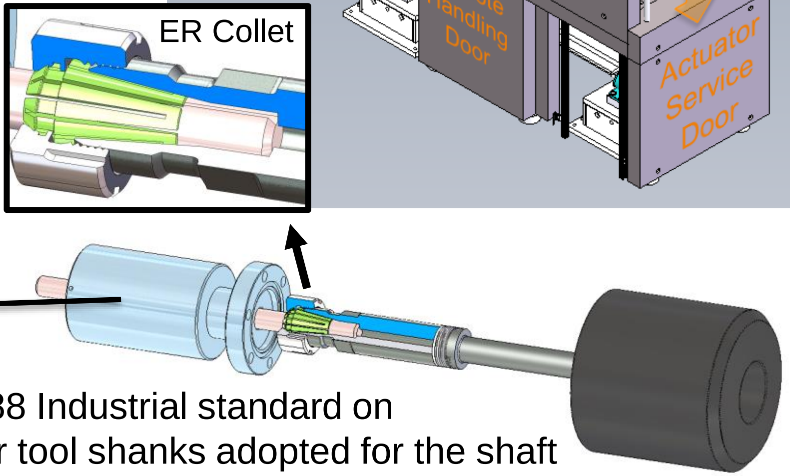

ISO 15488 Industrial standard on collets for tool shanks adopted for the shaft

Failure Mode, Prevention & Detection

- Failure Mode and Effects Analysis (FMEA) identified **brittle failure** of the graphite wheel as the highest risk scenario
- Mohr-Coulomb Failure Criterion (**Safety Factor = 3.6**)

Mohr-Coulomb Failure Criterion
Safety Factor

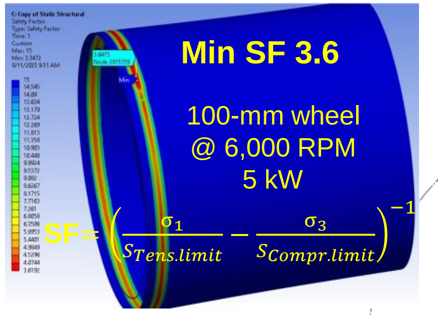

Minimum Principal Stress
(Compressive)

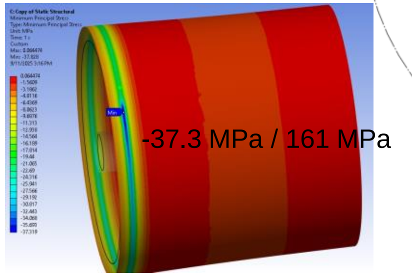

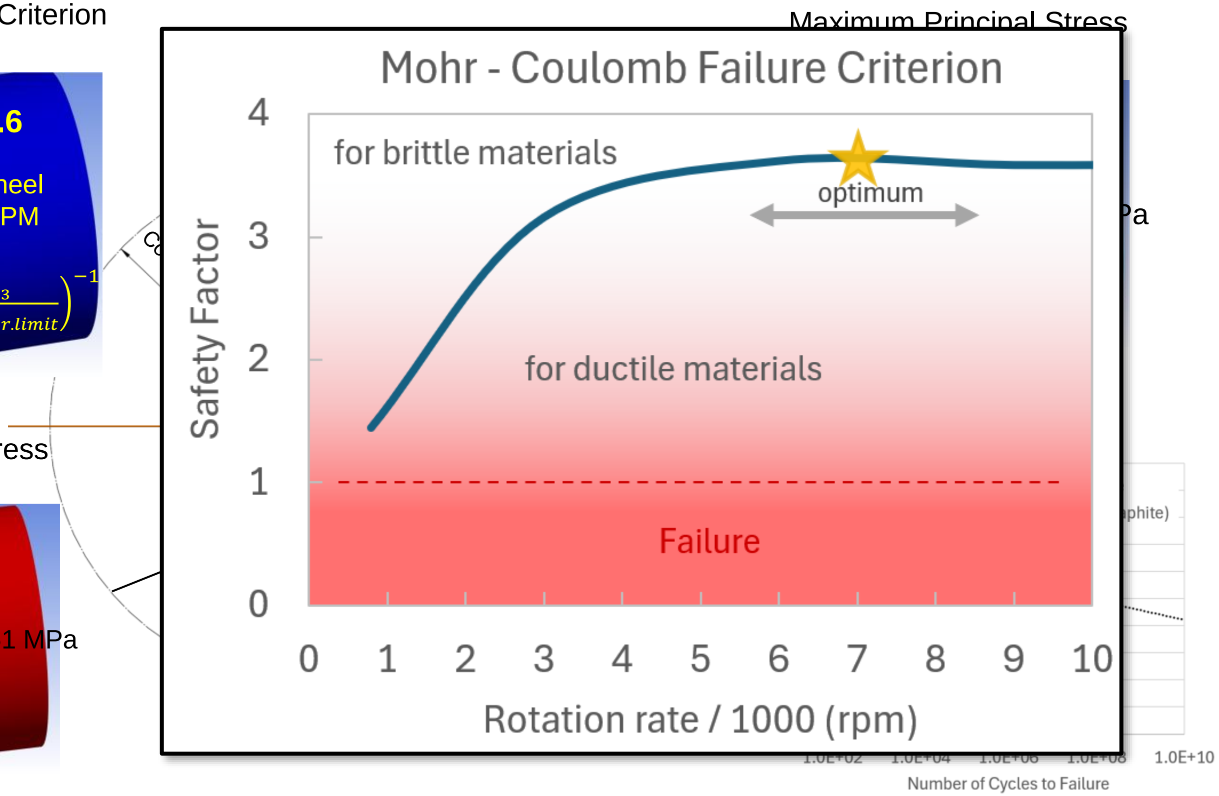

- **Prevention** and detection:
  - Design safety factor
  - Thermal imaging

  - Accelerometers (for vibration detection)
  - Photodiode (for fast response)
  - Catcher plate (to detect graphite failure and trip the beam)

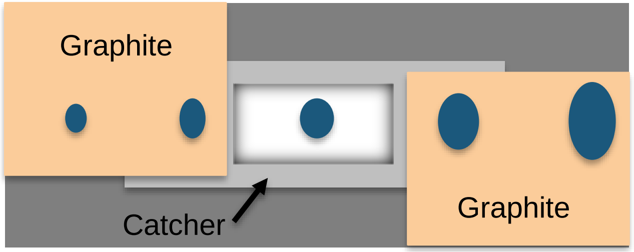

A Pile of Challenges

- The pile is a more comprehensive set of charge selector challenges
- Design of a charge selector is a multi-dimensional problem

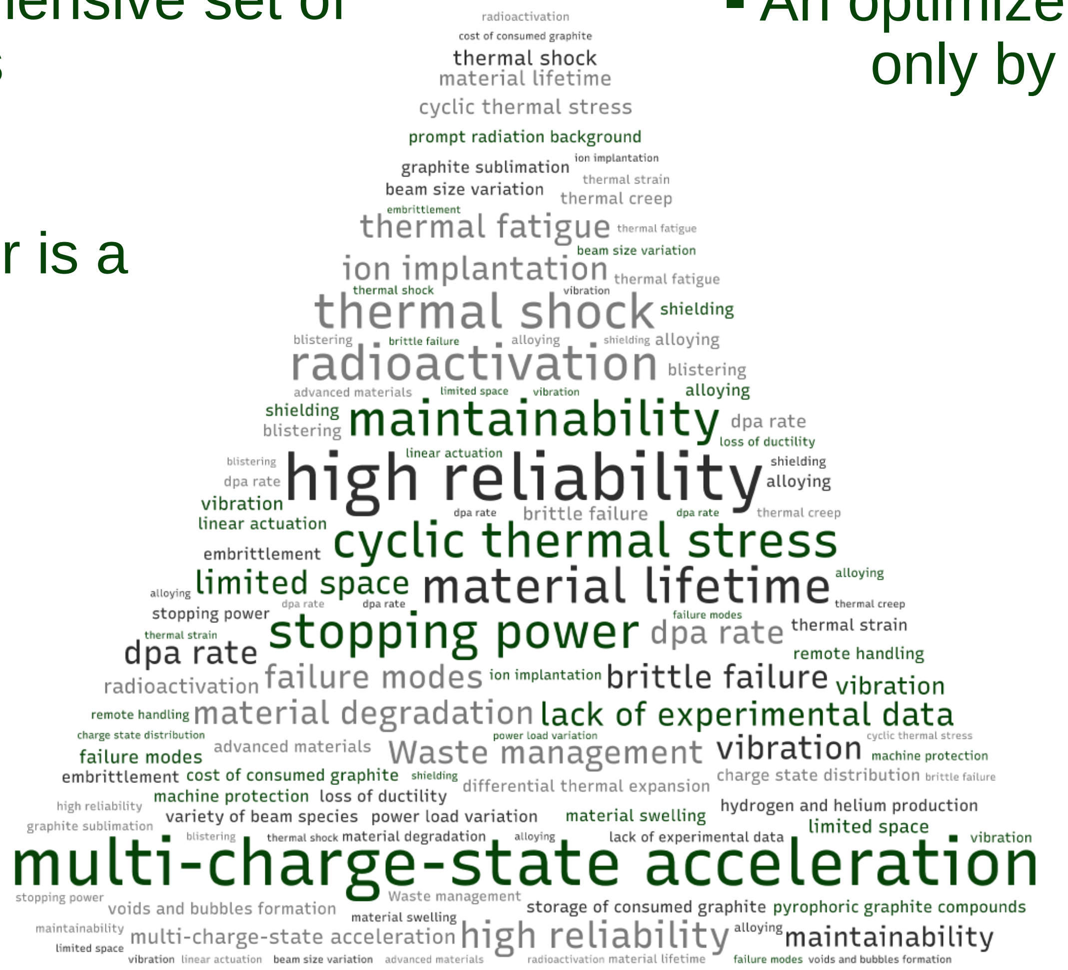

- An optimized design can be developed only by bringing together expertise from multiple scientific and engineering disciplines

Authors List

FRIB scientists and engineers supporting the charge selector design and operations:

- **High Power Targetry**
  - Basil Abdelmegied
  - Ethan Fletcher
  - Takuji Kanemura
  - Felix Marti
  - Eiichi Wakai
  - Xiuli Wang
  - Jie Wei
  - Lucas Zampieri
  - Qipei Zhong

- **Mechanical Engineering**
  - Nathan Bultman
  - Stefan Carter
  - Samuel Chrenka
  - Nicholas Jockheck
  - Michael LaVere
  - Samuel Miller
  - Mohit Patil
  - Raul Quispe-Abad
  - Daniel Simon

- **Remote Handling**
  - Michael Larmann

- **Accelerator Physics**
  - Peter Ostroumov
  - Alexander Plastun
  - Qiang Zhao

- **Instrumentation and Controls**
  - Francisco Pereira de Figueiredo
  - Igor Nesterenko

- **Radiation Transport**
  - Tom Ginter
  - Juan Carlos Zamora

Thank you!

Facility for Rare Isotope Beams
U.S. Department of Energy Office of Science | Michigan State University
640 South Shaw Lane • East Lansing, MI 48824, USA
frib.msu.edu